K. Shi, C. Liu, J.D. Biggs, Z. Sun, X. Yue
Observer-Based Control for Spacecraft Electromagnetic Docking
Aerospace Science and Technology, Vol. 99, 2020, 105759 (16 pages)
doi:10.1016/j.ast.2020.105759

Observer-Based Control for Spacecraft Electromagnetic Docking

Keke Shi[1], Chuang Liu[2,*], James D. Biggs[3], Zhaowei Sun[1], Xiaokui Yue[2]

1. Research Center of Satellite Technology, Harbin Institute of Technology, Harbin 150001, China

2. School of Astronautics, Northwestern Polytechnical University, Xi'an 710072, China

3. Department of Aerospace Science and Technology, Politecnico di Milano, Milano 20156, Italy

Abstract: Electromagnetic docking could enable autonomous spacecraft docking with no need for propellant consumption and without plume contamination. This paper addresses the robust electromagnetic docking problem for spacecraft in the presence of external disturbances, fault signals, unknown mass, elliptical eccentricity, measurement errors and input constraints. In this scenario, an intermediate observer is developed to estimate the relative motion information and the lumped disturbance resulting from these uncertainties. Based on this, an anti-disturbance controller is proposed, where the compensation of the lumped disturbance is considered. It is proved via Lyapunov analysis that the intermediate observer-based controller can achieve the objective of spacecraft electromagnetic docking with input constraints and in the presence of uncertainties. Finally, the observer-based controller is illustrated, in simulation, to demonstrate the effectiveness and improved performance compared with a disturbance observer-based controller.

Keywords: spacecraft electromagnetic docking, intermediate observer, unknown mass, measurement errors, input constraints

1. Introduction

Spacecraft electromagnetic docking is a novel technology that applies an inter-craft electromagnetic force, generated by magnetic coils equipped on the neighboring target and chaser spacecraft, to control the relative motion between them. Electromagnetic docking has distinct advantages over other docking mechanisms, for example, it does not require propellant, nor plume contamination, with continuous, reversible and non-contact actuation [1, 2]. However, along with these advantages come challenges related to its complex and coupled dynamics, uncertainties

* Corresponding author.
E-mail addresses: shikeke@hit.edu.cn (K. Shi), liuchuangforever@msn.com (C. Liu), jamesdouglas.biggs@polimi.it (J.D. Biggs), sunzhaowei@hit.edu.cn (Z. Sun), xkyue@nwpu.edu.cn (X. Yue)

that can influence the robust performance of the docking system.

Autonomous rendezvous and docking technologies for small spacecraft are necessary to enable on-orbit assembly schemes. Small spacecraft have the distinct advantages of low cost and weight, which make them particularly attractive to multi-agent missions such as on-orbit assembly. Non-contact docking uses the interaction of magnetic or electric fields generated by the spacecraft, including Coulomb force, electromagnetic force and flux-pinning force [3, 4]. According to [4] and [5], the Coulomb force is incapable of 6-DOF control, while flux-pinned space modules are passively stable only when the separation distance is on the order of 10 cm. Therefore, this paper focuses on the inter-craft electromagnetic forces. In spacecraft electromagnetic docking, each spacecraft is equipped with three large orthogonal coils that can generate electromagnetic forces. The relative positions between spacecraft are then determined by these electromagnetic forces, while the relative orientation of the dipoles on spacecraft is controlled using reaction wheels or control moment gyros to generate the counteracting torques [6]. The focus of this paper is on the position control problem of spacecraft electromagnetic docking in the presence of external disturbances, fault signals, unknown mass, elliptical eccentricity, measurement errors and input constraints.

The translational dynamics of a spacecraft using electromagnetic force are highly coupled and nonlinear, which increases the challenge for precise docking maneuvers. Most of the existing work in the field of electromagnetic docking only consider circular orbits of the spacecraft, which would fail in missions where the target spacecraft is in a large-eccentric orbit. Electromagnetic docking systems are also constrained by the maximum available current density of the electromagnetic coils [7,8]. Moreover, for traditional docking mechanisms the magnitude of order of the external disturbance is negligible over a short period of time, while electromagnetic forces increase as the relative distance decreases. Consequently, the external disturbance force and the electromagnetic force will be of the same magnitude of order when the relative distance is greater than a certain value. Since spacecraft electromagnetic docking technology has not been mature until now, controllers designed for fault-free cases may not be directly applicable to reality. In contrast to this, a fault tolerant controller can guarantee stability and performance in case of component fault/failure [9,10]. Thus, the possible fault signals should be taken into account in the controller design.

In addition to the problems mentioned, it is often expensive or even impossible to determine the mass properties of the spacecraft and this can lead to a loss of control precision. To alleviate this requirement, the controllers developed in [11] and [12] were inertia-free in the sense that no prior information on inertia matrix is required. Analogous to this, for electromagnetic docking missions, the controller developed in [8] required no mass information on the chaser

or target spacecraft, but the relative motion information should be accurately known. Various navigation sensors have been used to determine the target spacecraft's relative state using LIDAR, which inevitably have measurement errors that can lead to poorer control performance [13,14].

A challenging problem which arises in the domain of electromagnetic docking is that external disturbances, fault signals, mass properties and measurement errors may be unknown, which further increases the complexity of control design. Future space missions demand that the new generation of spacecraft should be able to perform on-orbit servicing missions with high precision and better robustness to inexact knowledge of spacecraft mass and other uncertainties. One way to overcome this problem is by using disturbance rejection control where the lumped disturbance is estimated and compensated for in the control [15]. Thus, disturbance observer-based control has been widely studied and explored in practical applications [16,17]. However, the state information and mass properties are often needed for control design.

To our knowledge, no study has explicitly focused on the aforementioned issues, i.e. external disturbances, fault signals, unknown mass, elliptical eccentricity, measurement errors and input constraints, in the case that the relative motion information on electromagnetic docking spacecraft is unavailable. These gaps make spacecraft electromagnetic docking much more difficult, but through the use of well-designed controllers and docking actuators these difficulties can be overcome. Thus, it is necessary to develop effective control schemes for spacecraft electromagnetic docking system in the presence of external disturbances, fault signals, unknown mass, elliptical eccentricity, measurement errors, and input constraints. The aim of this paper is to develop a novel intermediate observer-based control scheme without knowing exactly the external disturbances, fault signals, measurement errors and mass properties to achieve high-precision control of electromagnetic docking for spacecraft in elliptical orbits. The paper documents several key contributions made to the field of spacecraft electromagnetic docking. First, compared with [8], where the relative position and velocity are required to be measurable for direct feedback control, the control objective of spacecraft electromagnetic docking can be achieved if the relative position and velocity are unavailable. Second, compared with [12] and [18], where the observer and controller gains are independently given in advance according to Hurwitz stability theory, the observer and controller gains are obtained simultaneously by solving linear matrix inequalities (LMIs), with the input constraint satisfying given limits. As the observer and controller gains depend on each other for electromagnetic docking, the control strategy here has made the use of electromagnetic docking closer to realization compared with the state of the art. Third, compared with [11] and [19],

no parameter identifications and neural or fuzzy nonlinear approximations for the mass of chaser and target spacecraft are needed. Fourth, the developed control scheme is not only applicable to spacecraft electromagnetic docking systems subject to input constraints, but also easily extendable to a more general class of second-order system with input constraints. Here the lumped disturbance resulting from external disturbances, fault signals, unknown mass and elliptical eccentricity is addressed here for an anti-disturbance controller design, where an intermediate observer is developed to estimate the relative motion information and the lumped disturbance.

The rest of this paper is organized as follows. The next section focuses on the mathematic models for electromagnetic docking systems of the chaser and target spacecraft, where external disturbances, fault signals, unknown mass, elliptical eccentricity and measurement errors are taken into account, and the corresponding control problem is formulated. Then, the main results of this work are presented, where a novel intermediate observer-based control scheme with input constraints is proposed, and the corresponding stability analysis is performed via a Lyapunov approach. It is followed by the numerical simulations to demonstrate the performance and superiority of the proposed control strategy. Finally, conclusions are drawn.

2. Problem formulation

2.1. Dynamic Modeling

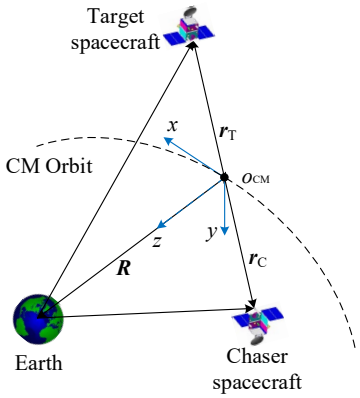

Fig.1 Spacecraft docking system

The center of mass of the spacecraft electromagnetic docking system is denoted by ‘CM’. The relevant coordinate system adopted for spacecraft electromagnetic docking missions is the orbital reference frame shown in Fig.1, where the origin is attached to ‘CM’ with z-axis pointing radially toward the Earth’s center, x-axis is perpendicular to z-axis in the nominal direction of flight, and y-axis completes the right-handed coordinate system. The motion of frame $o_{CM}xyz$ is not influenced by electromagnetic force and thus it could be hypothesized as a reference frame, where the dynamic

models are developed. The relative motions satisfy constraint conditions based on Clohessy-Wiltshire (CW) equations, extending them to an eccentric orbit by using the true anomaly of 'CM' gives the dynamic models of chaser and target spacecraft relative to 'CM' expressed by Eqs.(1) and (2) respectively.

$$\begin{cases} \ddot{x}_{\mathrm{C}} - \omega^2 x_{\mathrm{C}} - 2\omega\dot{z}_{\mathrm{C}} - \dot{\omega} z_{\mathrm{C}} = -\dfrac{\mu x_{\mathrm{C}}}{\left\|\boldsymbol{R}+\boldsymbol{r}_{\mathrm{C}}\right\|^3} + \dfrac{F_{\mathrm{eC}x}}{m_{\mathrm{C}}} + \dfrac{w_{\mathrm{C}x}}{m_{\mathrm{C}}} \\ \ddot{y}_{\mathrm{C}} = -\dfrac{\mu y_{\mathrm{C}}}{\left\|\boldsymbol{R}+\boldsymbol{r}_{\mathrm{C}}\right\|^3} + \dfrac{F_{\mathrm{eC}y}}{m_{\mathrm{C}}} + \dfrac{w_{\mathrm{C}y}}{m_{\mathrm{C}}} \\ \ddot{z}_{\mathrm{C}} - \omega^2 z_{\mathrm{C}} + 2\omega\dot{x}_{\mathrm{C}} + \dot{\omega} x_{\mathrm{C}} = \dfrac{2\mu z_{\mathrm{C}}}{\left\|\boldsymbol{R}+\boldsymbol{r}_{\mathrm{C}}\right\|^3} + \dfrac{F_{\mathrm{eC}z}}{m_{\mathrm{C}}} + \dfrac{w_{\mathrm{C}z}}{m_{\mathrm{C}}} \end{cases} \tag{1}$$

$$\begin{cases} \ddot{x}_{\mathrm{T}} - \omega^2 x_{\mathrm{T}} - 2\omega\dot{z}_{\mathrm{T}} - \dot{\omega} z_{\mathrm{T}} = -\dfrac{\mu x_{\mathrm{T}}}{\left\|\boldsymbol{R}+\boldsymbol{r}_{\mathrm{T}}\right\|^3} - \dfrac{F_{\mathrm{eT}x}}{m_{\mathrm{T}}} + \dfrac{w_{\mathrm{T}x}}{m_{\mathrm{T}}} \\ \ddot{y}_{\mathrm{T}} = -\dfrac{\mu y_{\mathrm{T}}}{\left\|\boldsymbol{R}+\boldsymbol{r}_{\mathrm{T}}\right\|^3} + \dfrac{F_{\mathrm{eT}y}}{m_{\mathrm{T}}} + \dfrac{w_{\mathrm{T}y}}{m_{\mathrm{T}}} \\ \ddot{z}_{\mathrm{T}} - \omega^2 z_{\mathrm{T}} + 2\omega\dot{x}_{\mathrm{T}} + \dot{\omega} x_{\mathrm{T}} = \dfrac{2\mu z_{\mathrm{T}}}{\left\|\boldsymbol{R}+\boldsymbol{r}_{\mathrm{T}}\right\|^3} + \dfrac{F_{\mathrm{eT}z}}{m_{\mathrm{T}}} + \dfrac{w_{\mathrm{T}z}}{m_{\mathrm{T}}} \end{cases} \tag{2}$$

with

$$\omega = \frac{(1+e\cos\theta)^2}{(1-e^2)^{3/2}}\sqrt{\frac{\mu}{a^3}}, \quad R = \frac{a(1-e^2)}{1+e\cos\theta} \tag{3}$$

where, θ is the true anomaly, e and a are the eccentricity and semi-major axis of 'CM' orbit; $\omega = \dot{\theta}$ is the orbital frequency of 'CM' and μ is the gravitational parameter; m_{C} and m_{T} represent the mass of the chaser and target spacecraft; $\boldsymbol{r}_{\mathrm{C}} = \begin{bmatrix} x_{\mathrm{C}} & y_{\mathrm{C}} & z_{\mathrm{C}} \end{bmatrix}^{\mathrm{T}}$ and $\boldsymbol{r}_{\mathrm{T}} = \begin{bmatrix} x_{\mathrm{T}} & y_{\mathrm{T}} & z_{\mathrm{T}} \end{bmatrix}^{\mathrm{T}}$ denote the relative position vectors from 'CM' to the chaser and target spacecraft, according to the definition of 'CM' point, we know $m_{\mathrm{C}}(\boldsymbol{R}+\boldsymbol{r}_{\mathrm{C}}) + m_{\mathrm{T}}(\boldsymbol{R}+\boldsymbol{r}_{\mathrm{T}}) = (m_{\mathrm{C}}+m_{\mathrm{T}})\boldsymbol{R}$, thus $m_{\mathrm{C}}\boldsymbol{r}_{\mathrm{C}} = -m_{\mathrm{T}}\boldsymbol{r}_{\mathrm{T}}$; $\boldsymbol{R}$ represents the position vector from the center of Earth to 'CM', with $R = \left\|\boldsymbol{R}\right\|$ as 'CM' orbit radius and $\left\|\cdot\right\|$ denotes 2-norm; $F_{\mathrm{eC}i}$ and $F_{\mathrm{eT}i}$ (i=x,y,z) denote the ith component of electromagnetic forces acting on the two spacecraft with $F_{\mathrm{eT}i} = -F_{\mathrm{eC}i}$; $w_{\mathrm{C}i}$ and $w_{\mathrm{T}i}$ (i=x,y,z) are the ith component of external disturbances acting on the chaser and target spacecraft.

The external disturbances acting on the chaser and target spacecraft are often generated due to many factors. For example, the gradient of the geomagnetic field strength gives the force on the two spacecraft due to the geomagnetic field, which is due to the core of the planet and can be described as a combination of main field. In addition, an external

component (that can be as much as 10% of the main field) often exist, which is due to sources such as ionosphere and solar wind effects on the Earth's magnetosphere.

Denoting $\tilde{\boldsymbol{\eta}} = \begin{bmatrix} x & y & z \end{bmatrix}^{\mathrm{T}}$ as the relative position vector from target to chaser spacecraft, i.e. $\tilde{\boldsymbol{\eta}} = \boldsymbol{r}_{\mathrm{C}} - \boldsymbol{r}_{\mathrm{T}}$ and $\|\tilde{\boldsymbol{\eta}}\| = \|\boldsymbol{r}_{\mathrm{C}}\| + \|\boldsymbol{r}_{\mathrm{T}}\|$, with Eqs.(1) and (2), we have

$$\begin{cases} \ddot{x} - \omega^2 x - 2\omega\dot{z} - \dot{\omega} z = -\dfrac{\mu x_{\mathrm{C}}}{\|\boldsymbol{R} + \boldsymbol{r}_{\mathrm{C}}\|^3} + \dfrac{\mu x_{\mathrm{T}}}{\|\boldsymbol{R} + \boldsymbol{r}_{\mathrm{T}}\|^3} + \dfrac{F_{\mathrm{eC}x}}{m_{\mathrm{C}}} + \dfrac{F_{\mathrm{eC}x}}{m_{\mathrm{T}}} + \dfrac{w_{\mathrm{C}x}}{m_{\mathrm{C}}} - \dfrac{w_{\mathrm{T}x}}{m_{\mathrm{T}}} \\ \ddot{y} = -\dfrac{\mu y_{\mathrm{C}}}{\|\boldsymbol{R} + \boldsymbol{r}_{\mathrm{C}}\|^3} + \dfrac{\mu y_{\mathrm{T}}}{\|\boldsymbol{R} + \boldsymbol{r}_{\mathrm{T}}\|^3} + \dfrac{F_{\mathrm{eC}y}}{m_{\mathrm{C}}} + \dfrac{F_{\mathrm{eC}y}}{m_{\mathrm{T}}} + \dfrac{w_{\mathrm{C}y}}{m_{\mathrm{C}}} - \dfrac{w_{\mathrm{T}y}}{m_{\mathrm{T}}} \\ \ddot{z} - \omega^2 z + 2\omega\dot{x} + \dot{\omega} x = \dfrac{2\mu z_{\mathrm{C}}}{\|\boldsymbol{R} + \boldsymbol{r}_{\mathrm{C}}\|^3} - \dfrac{2\mu z_{\mathrm{T}}}{\|\boldsymbol{R} + \boldsymbol{r}_{\mathrm{T}}\|^3} + \dfrac{F_{\mathrm{eC}z}}{m_{\mathrm{C}}} + \dfrac{F_{\mathrm{eC}z}}{m_{\mathrm{T}}} + \dfrac{w_{\mathrm{C}z}}{m_{\mathrm{C}}} - \dfrac{w_{\mathrm{T}z}}{m_{\mathrm{T}}} \end{cases} \tag{4}$$

For small relative distance between the chaser and target spacecraft in comparison with 'CM' orbit radius, i.e. $\|\tilde{\boldsymbol{\eta}}\| \ll R$, Eq.(4) can be converted into

$$\begin{cases} \ddot{x} - \omega^2 x - 2\omega\dot{z} - \dot{\omega} z = -\dfrac{\mu x}{R^3} + \dfrac{1}{m_{\mathrm{CT}}}\left(F_{\mathrm{eC}x} + d_x\right) \\ \ddot{y} = -\dfrac{\mu y}{R^3} + \dfrac{1}{m_{\mathrm{CT}}}\left(F_{\mathrm{eC}y} + d_y\right) \\ \ddot{z} - \omega^2 z + 2\omega\dot{x} + \dot{\omega} x = \dfrac{2\mu z}{R^3} + \dfrac{1}{m_{\mathrm{CT}}}\left(F_{\mathrm{eC}z} + d_z\right) \end{cases} \tag{5}$$

where, $m_{\mathrm{CT}} = \dfrac{m_{\mathrm{C}} m_{\mathrm{T}}}{m_{\mathrm{C}} + m_{\mathrm{T}}}$, $d_{i=x,y,z} = \dfrac{m_{\mathrm{T}} w_{\mathrm{C}i} - m_{\mathrm{C}} w_{\mathrm{T}i}}{m_{\mathrm{C}} + m_{\mathrm{T}}}$.

By approximating the coils on each spacecraft to a steerable dipole, the electromagnetic force between the two spacecraft can be written as [20]

$$\boldsymbol{F}_{e\mathrm{C}} = \frac{3\mu_0}{4\pi}\left[\frac{1}{\|\tilde{\boldsymbol{\eta}}\|^5}\left((\boldsymbol{\mu}_{\mathrm{T}} \cdot \boldsymbol{\mu}_{\mathrm{C}})\tilde{\boldsymbol{\eta}} + (\boldsymbol{\mu}_{\mathrm{T}} \cdot \tilde{\boldsymbol{\eta}})\boldsymbol{\mu}_{\mathrm{C}} + (\boldsymbol{\mu}_{\mathrm{C}} \cdot \tilde{\boldsymbol{\eta}})\boldsymbol{\mu}_{\mathrm{T}}\right) - \frac{5}{\|\tilde{\boldsymbol{\eta}}\|^7}(\boldsymbol{\mu}_{\mathrm{T}} \cdot \tilde{\boldsymbol{\eta}})(\boldsymbol{\mu}_{\mathrm{C}} \cdot \tilde{\boldsymbol{\eta}})\tilde{\boldsymbol{\eta}}\right] \tag{6}$$

where $\boldsymbol{F}_{e\mathrm{C}}$ denotes the electromagnetic force on the dipole present on chaser spacecraft due to the dipole located on target spacecraft; μ_0 is the permeability of free space, $\boldsymbol{\mu}_{\mathrm{C}}$ and $\boldsymbol{\mu}_{\mathrm{T}}$ are magnetic moment vectors of the chaser and target spacecraft respectively.

It should be noted that the magnetic moment vectors $\boldsymbol{\mu}_{\mathrm{C,T}}$ are defined as

$$\boldsymbol{\mu}_{\mathrm{C,T}} = NiS\hat{\boldsymbol{n}} \tag{7}$$

where, N is the number of coil turns, i is the current passing through the coil, S is the coil cross-sectional area and $\hat{\boldsymbol{n}}$ is oriented so as to respect the right hand rule.

Furthermore, Eq.(6) is equivalent to

$$\begin{aligned}\boldsymbol{F}_{e\mathrm{C}} &= \frac{3\mu_0}{4\pi}\left[\frac{1}{\|\tilde{\boldsymbol{\eta}}\|^5}\left(\tilde{\boldsymbol{\eta}}(\boldsymbol{\mu}_{\mathrm{T}}^{\mathrm{T}}\boldsymbol{\mu}_{\mathrm{C}})+(\boldsymbol{\mu}_{\mathrm{T}}^{\mathrm{T}}\tilde{\boldsymbol{\eta}})\boldsymbol{\mu}_{\mathrm{C}}+\boldsymbol{\mu}_{\mathrm{T}}(\tilde{\boldsymbol{\eta}}^{\mathrm{T}}\boldsymbol{\mu}_{\mathrm{C}})\right)-\frac{5}{\|\tilde{\boldsymbol{\eta}}\|^7}\tilde{\boldsymbol{\eta}}(\boldsymbol{\mu}_{\mathrm{T}}^{\mathrm{T}}\tilde{\boldsymbol{\eta}})(\tilde{\boldsymbol{\eta}}^{\mathrm{T}}\boldsymbol{\mu}_{\mathrm{C}})\right] \\ &= \frac{3\mu_0}{4\pi}\left[\frac{1}{\|\tilde{\boldsymbol{\eta}}\|^5}(\tilde{\boldsymbol{\eta}}\boldsymbol{\mu}_{\mathrm{T}}^{\mathrm{T}}+\boldsymbol{\mu}_{\mathrm{T}}^{\mathrm{T}}\tilde{\boldsymbol{\eta}}\boldsymbol{I}_3+\boldsymbol{\mu}_{\mathrm{T}}\tilde{\boldsymbol{\eta}}^{\mathrm{T}})-\frac{5}{\|\tilde{\boldsymbol{\eta}}\|^7}\tilde{\boldsymbol{\eta}}\boldsymbol{\mu}_{\mathrm{T}}^{\mathrm{T}}\tilde{\boldsymbol{\eta}}\tilde{\boldsymbol{\eta}}^{\mathrm{T}}\right]\boldsymbol{\mu}_{\mathrm{C}} \\ &= \frac{3\mu_0}{4\pi}\boldsymbol{\Xi}(\boldsymbol{\mu}_{\mathrm{T}},\tilde{\boldsymbol{\eta}})\boldsymbol{\mu}_{\mathrm{C}}\end{aligned} \tag{8}$$

where,

$$\boldsymbol{\Xi}(\boldsymbol{\mu}_{\mathrm{T}},\tilde{\boldsymbol{\eta}})=\frac{1}{\|\tilde{\boldsymbol{\eta}}\|^5}(\tilde{\boldsymbol{\eta}}\boldsymbol{\mu}_{\mathrm{T}}^{\mathrm{T}}+\boldsymbol{\mu}_{\mathrm{T}}^{\mathrm{T}}\tilde{\boldsymbol{\eta}}\boldsymbol{I}_3+\boldsymbol{\mu}_{\mathrm{T}}\tilde{\boldsymbol{\eta}}^{\mathrm{T}})-\frac{5}{\|\tilde{\boldsymbol{\eta}}\|^7}\tilde{\boldsymbol{\eta}}\boldsymbol{\mu}_{\mathrm{T}}^{\mathrm{T}}\tilde{\boldsymbol{\eta}}\tilde{\boldsymbol{\eta}}^{\mathrm{T}}$$

The far-field model, i.e. Eq.(6), of electromagnetic force is derived based on the dipole hypothesis. It is only accurate when the relative distance between the two spacecraft is not less than a certain threshold, which is related to the mechanism configuration, such as 6-8 times the coil radius, as described in [2] and [20]. When the two spacecraft are very close to each other, the resulting error from far-field model can be regarded as a source to external disturbances. Due to inherent nonlinearities and couplings, the dynamics and control problems associated with electromagnetic docking are difficult, especially for elliptical orbit. Thus, the electromagnetic force can be firstly regarded as the control input, which will result in the solution of magnetic moments with details below. As the information on relative motion, i.e. $\tilde{\boldsymbol{\eta}}$, can be obtained at each time instant, so that the matrix $\boldsymbol{\Xi}(\boldsymbol{\mu}_{\mathrm{T}},\tilde{\boldsymbol{\eta}})$ will be calculated. According to Eq.(8), the solution of the magnetic moment vector of chaser spacecraft can be calculated via the electromagnetic force $\boldsymbol{F}_{e\mathrm{C}}$ and the matrix $\boldsymbol{\Xi}(\boldsymbol{\mu}_{\mathrm{T}},\tilde{\boldsymbol{\eta}})$.

With Eq.(3), Eq.(5) can be converted into the following state-space form:

$$\begin{cases}\dot{\boldsymbol{\eta}}(t)=(\boldsymbol{A}+\boldsymbol{\Delta A})\boldsymbol{\eta}(t)+(\boldsymbol{B}+\boldsymbol{\Delta B})(\boldsymbol{u}(t)+\boldsymbol{w}_0(t)) \\ \boldsymbol{y}(t)=\boldsymbol{C}\boldsymbol{\eta}(t)\end{cases} \tag{9}$$

where $\boldsymbol{\eta}=[x \quad y \quad z \quad \dot{x} \quad \dot{y} \quad \dot{z}]^{\mathrm{T}}$ is the state vector, $\boldsymbol{y}=[x \quad y \quad z \quad \dot{x} \quad \dot{y} \quad \dot{z}]^{\mathrm{T}}$ is the output vector, $\boldsymbol{u}=\begin{bmatrix}F_{\mathrm{eC}x} & F_{\mathrm{eC}y} & F_{\mathrm{eC}z}\end{bmatrix}^{\mathrm{T}}$ is the control force, $\boldsymbol{w}_0=\begin{bmatrix}d_x & d_y & d_z\end{bmatrix}^{\mathrm{T}}$ is the external disturbance. The known coefficient matrices are denoted by

$$\boldsymbol{A}=\begin{bmatrix} 0 & 0 & 0 & 1 & 0 & 0 \\ 0 & 0 & 0 & 0 & 1 & 0 \\ 0 & 0 & 0 & 0 & 0 & 1 \\ 0 & 0 & 0 & 0 & 0 & 2\omega_0 \\ 0 & -\omega_0^2 & 0 & 0 & 0 & 0 \\ 0 & 0 & 3\omega_0^2 & -2\omega_0 & 0 & 0 \end{bmatrix}$$

$$\boldsymbol{B}=\left[\boldsymbol{0}_{3\times 3} \quad \mathrm{diag}(m_0^{-1}, m_0^{-1}, m_0^{-1})\right]^{\mathrm{T}}, \boldsymbol{C}=\boldsymbol{I}_{6\times 6}$$

and the unknown coefficient matrices are denoted by

$$\Delta\boldsymbol{A}=\begin{bmatrix} 0 & 0 & 0 & 0 & 0 & 0 \\ 0 & 0 & 0 & 0 & 0 & 0 \\ 0 & 0 & 0 & 0 & 0 & 0 \\ \dfrac{e\cos\theta}{1+e\cos\theta}\omega^2 & 0 & \dot{\omega} & 0 & 0 & 2(\omega-\omega_0) \\ 0 & \omega_0^2-\omega^2 & 0 & 0 & 0 & 0 \\ -\dot{\omega} & 0 & \dfrac{3+e\cos\theta}{1+e\cos\theta}\omega^2-3\omega_0^2 & 2(\omega_0-\omega) & 0 & 0 \end{bmatrix}$$

$$\Delta\boldsymbol{B}=\left[\boldsymbol{0}_{3\times 3} \quad \mathrm{diag}(m_{\mathrm{CT}}^{-1}-m_0^{-1}, m_{\mathrm{CT}}^{-1}-m_0^{-1}, m_{\mathrm{CT}}^{-1}-m_0^{-1})\right]^{\mathrm{T}}$$

where $\omega_0=\sqrt{\mu/a^3}$ and m_0 is only representative of a valid mass.

In addition, the following important points should be noted.

1) Measurement errors

The output model in Eq.(9) is based upon the assumption that true position and velocity states of the spacecraft are known, but in any real case, only the sensor measurement derived estimates for spacecraft states are available for feedback purposes. Hence, the sensor measurement error $\boldsymbol{v}(t)\in L_2\left[0,+\infty\right)$ may appear that represents an aggregation of sensor calibration errors, systematic bias in errors, and some stochastic disturbances present in any real sensor measurement.

2) Actuator faults

Since the performance of a spacecraft docking system can be severely impaired by improper actuator actions, actuator fault has been considered to be one of the most critical challenges to be solved [21]. Taking this issue into account, let $\boldsymbol{E}$ with full-column rank, which has similar structure with $\boldsymbol{B}$, denote the distribution matrix of fault signals $\boldsymbol{f}(t)$ appearing in the input. Specifically, it represents the process fault if $\boldsymbol{E}\neq\boldsymbol{B}$, and it also represents the actuator fault if $\boldsymbol{E}=\boldsymbol{B}$.

3) Actuator saturation

Due to the maximum available current density of the electromagnetic coils and other physical limitations, the actuator constraint, if unaccounted for, will often have a negative impact on the stability and performance of an electromagnetic docking system designed for the "ideal" case. In order not to violate the requirements necessary for input constraints, a positive scalar λ is introduced satisfying

$$\|\boldsymbol{u}\| < \lambda \tag{10}$$

where λ denotes the 2-norm of control input.

In other cases, when the electromagnetic docking system works, if the theoretical control force is larger than the saturation value of actual control force, the actual control force $sat(\boldsymbol{u})$ should be described as[22]

$$\mathrm{sat}(u_{i=1,2,3}(t)) = \mathrm{sign}(u_i(t)) \min\left\{\left|u_i(t)\right|, u_{mi}\right\} \tag{11}$$

where u_{mi} is the upper boundary of control input that the actuator can provide.

Considering the above factors, the new form of spacecraft electromagnetic docking system can be expressed as:

$$\begin{cases} \dot{\boldsymbol{\eta}}(t) = \boldsymbol{A}\boldsymbol{\eta}(t) + \boldsymbol{B}\boldsymbol{u}(t) + \boldsymbol{B}\boldsymbol{w}(t) \\ \boldsymbol{y}(t) = \boldsymbol{C}\boldsymbol{\eta}(t) + \boldsymbol{v}(t) \end{cases} \tag{12}$$

where $\boldsymbol{w}(t)=\boldsymbol{B}^{\mathrm{T}}(\boldsymbol{B}\boldsymbol{B}^{\mathrm{T}})^{*}\left(\boldsymbol{\Delta A}\boldsymbol{\eta}(t) + \boldsymbol{\Delta B}\boldsymbol{u}(t) + (\boldsymbol{B}+\boldsymbol{\Delta B})\boldsymbol{w}_0(t) + \boldsymbol{E}\boldsymbol{f}(t)\right)$ is regarded as the lumped disturbance from external disturbances, fault signals, unknown mass and elliptical eccentricity, and where the matrix $(\boldsymbol{B}\boldsymbol{B}^{\mathrm{T}})^{*}$ is the pseudoinverse of $\boldsymbol{B}\boldsymbol{B}^{\mathrm{T}}$.

Remark 1: The development of controllers for spacecraft electromagnetic docking is a labor-intensive, time-consuming process. In addition, it is often expensive to determine the mass properties with high precision. Hence, the nominal representative of a valid mass m_0 is used for the controller design, then the difference between m_0 and m_{CT} will appear. In other words, the influence of the eccentricity e and m_{CT} results in the appearance of $\boldsymbol{\Delta A}$ and $\boldsymbol{\Delta B}$, respectively. It is noted that the difference between m_0 and m_{CT} only affects the relative velocity, i.e. $\dot{x}$, $\dot{y}$ and $\dot{z}$. Thus, the combined uncertain term, i.e. $\boldsymbol{\Delta A}\boldsymbol{\eta}(t) + \boldsymbol{\Delta B}\boldsymbol{u}(t) + \boldsymbol{\Delta B}\boldsymbol{w}_0(t)$, will contribute to the disturbance, and the same applies to $\boldsymbol{E}\boldsymbol{f}(t)$. Together they form the lumped disturbance $\boldsymbol{w}(t)$.

2.2. Preliminaries

The subsection presents the following necessary assumptions, remarks and lemmas, which are needed to provide theoretical support before further analysis.

Assumption 1: The disturbance force $\boldsymbol{w}_0(t)$ and its first time derivative are assumed to be piecewise continuous and bounded.

Remark 2: Assumption 1 is reasonable. The main reason is that the external disturbances are primarily caused by solar radiation, geopotential anomaly, magnetic effects, and residual atmosphere, which are all continuous and bounded [23, 24]. In addition, because the total control authority is limited, all three available control input forces should be continuous and bounded, which is reasonable in practice. It is worth noting that the desired translational motion represented by relative position and velocity is also bounded and differentiable in practice. In particular, the derivative of $\boldsymbol{f}$(t) with respect to time is often assumed to be norm bounded [25]. They together result in the fact that the lumped disturbance force is bounded and differentiable, and the first derivative of $\boldsymbol{w}(t)$ satisfies $\|\dot{\boldsymbol{w}}(t)\| \le \kappa_1$, where $\kappa_1 \ge 0$. It should be noted that the norm of lumped disturbance $\boldsymbol{w}(t)$ and its components could be unknown. Thus, it is more general than the fault-tolerant sliding-mode-observer method in [26], which requires the preliminary knowledge of the bound of fault signals.

Assumption 2: The measurement error signal $\boldsymbol{v}(t)$ satisfies $\|\boldsymbol{v}(t)\| \le \kappa_2$ with $\kappa_2 \ge 0$, which describes the boundary of measurement errors.

Remark 3: Assumption 2 is common in literature [13, 27]. For κ_2 could be unknown when H_∞ control method is applied, it is more general compared with [27] where κ_2 should be known.

Assumption 3: $rank(\boldsymbol{B}, \boldsymbol{E}) = rank(\boldsymbol{B})$, and there exists a matrix $\boldsymbol{B}^*$ such that $(\boldsymbol{I} - \boldsymbol{B}\boldsymbol{B}^*)\boldsymbol{E} = 0$.

Remark 4: Assumption 3 is general in [28], which means that the faults appear in the actuator and can be compensated for by the control input.

Lemma 1 [12] (Schur complement lemma) Let the partitioned matrix

$$\boldsymbol{A} = \begin{bmatrix} \boldsymbol{A}_{11} & \boldsymbol{A}_{12} \\ * & \boldsymbol{A}_{22} \end{bmatrix}$$

be symmetric. Then

$$\boldsymbol{A} < 0 \Leftrightarrow \boldsymbol{A}_{11} < 0, \boldsymbol{A}_{22} - \boldsymbol{A}_{12}^{\mathrm{T}} \boldsymbol{A}_{11}^{-1} \boldsymbol{A}_{12} < 0 \Leftrightarrow \boldsymbol{A}_{22} < 0, \boldsymbol{A}_{11} - \boldsymbol{A}_{12} \boldsymbol{A}_{22}^{-1} \boldsymbol{A}_{12}^{\mathrm{T}} < 0$$

2.3. Control Objectives

Based on the spacecraft electromagnetic docking model governed by Eq.(12), one should design an effective control scheme to achieve the following objectives: a) the states of the closed-loop system are stabilized in the presence of external disturbances, fault signals, unknown mass, elliptical eccentricity, measurement errors and input constraints; b) the input constraint, i.e. $\|\boldsymbol{u}\| < \lambda$ is satisfied, where λ is a known positive constant; c) the relative motion information as well as the lumped disturbance are estimated with high precision.

3. Controller design

In this section, the relative motion information as well as the lumped disturbance should be estimated simultaneously such that the control scheme is designed based on the estimation. These requirements frequently necessitate the use of an intermediate variable for observer design. The new variable is described as

$$\boldsymbol{\xi}(t) = \boldsymbol{w}(t) - \varpi \boldsymbol{B}^{\mathrm{T}} \boldsymbol{\eta}(t) \tag{13}$$

$$\dot{\boldsymbol{\xi}}(t) = \dot{\boldsymbol{w}}(t) - \varpi \boldsymbol{B}^{\mathrm{T}} \left[\boldsymbol{A}\boldsymbol{\eta}(t) + \boldsymbol{B}\boldsymbol{u}(t) + \boldsymbol{B}\boldsymbol{\xi}(t) + \varpi \boldsymbol{B}\boldsymbol{B}^{\mathrm{T}} \boldsymbol{\eta}(t) \right] \tag{14}$$

For $\boldsymbol{w}(t)$ and $\boldsymbol{\eta}(t)$ are both bounded, the intermediate variable $\boldsymbol{\xi}(t)$ is also bounded, which satisfies $\|\boldsymbol{\xi}(t)\| \le \kappa_3$ with $\kappa_3 > 0$. Then, the intermediate observer is designed based on

$$\dot{\hat{\boldsymbol{\eta}}}(t) = \boldsymbol{A}\hat{\boldsymbol{\eta}}(t) + \boldsymbol{B}\boldsymbol{u}(t) + \boldsymbol{B}\hat{\boldsymbol{w}}(t) + \boldsymbol{L}(\boldsymbol{y}(t) - \hat{\boldsymbol{y}}(t)) \tag{15}$$

$$\dot{\hat{\boldsymbol{\xi}}}(t) = -\varpi \boldsymbol{B}^{\mathrm{T}} \left[\boldsymbol{A}\hat{\boldsymbol{\eta}}(t) + \boldsymbol{B}\boldsymbol{u}(t) + \boldsymbol{B}\hat{\boldsymbol{\xi}}(t) + \varpi \boldsymbol{B}\boldsymbol{B}^{\mathrm{T}} \hat{\boldsymbol{\eta}}(t) \right] \tag{16}$$

$$\hat{\boldsymbol{y}}(t) = \boldsymbol{C}\hat{\boldsymbol{\eta}}(t) \tag{17}$$

$$\hat{\boldsymbol{w}}(t) = \hat{\boldsymbol{\xi}}(t) + \varpi \boldsymbol{B}^{\mathrm{T}} \hat{\boldsymbol{\eta}}(t) \tag{18}$$

where $\hat{\boldsymbol{\eta}}(t)$, $\hat{\boldsymbol{\xi}}(t)$, $\hat{\boldsymbol{y}}(t)$ and $\hat{\boldsymbol{w}}(t)$ are the estimates of $\boldsymbol{\eta}(t)$, $\boldsymbol{\xi}(t)$, $\boldsymbol{y}(t)$ and $\boldsymbol{w}(t)$ respectively.

Based on the above estimations, the anti-disturbance controller is designed as

$$\boldsymbol{u}(t) = -\boldsymbol{K}\hat{\boldsymbol{\eta}}(t) - \hat{\boldsymbol{w}}(t) \tag{19}$$

where $\boldsymbol{K}$ is the controller gain matrix and $\hat{\boldsymbol{w}}(t)$ is added to the input to compensate for the effect of the lumped disturbance.

Denote $\boldsymbol{e}_{\eta}(t) = \boldsymbol{\eta}(t) - \hat{\boldsymbol{\eta}}(t)$ and $\boldsymbol{e}_{\xi}(t) = \boldsymbol{\xi}(t) - \hat{\boldsymbol{\xi}}(t)$, substituting Eq. (19) into the first of Eq. (12) yields

$$\dot{\boldsymbol{\eta}}(t) = (\boldsymbol{A} - \boldsymbol{B}\boldsymbol{K})\boldsymbol{\eta}(t) + \boldsymbol{B}\boldsymbol{K}e_{\eta}(t) + \boldsymbol{B}\boldsymbol{e}_{\boldsymbol{\xi}}(t) + \varpi \boldsymbol{B}\boldsymbol{B}^{\mathrm{T}} \boldsymbol{e}_{\eta}(t) \tag{20}$$

Then, it can be concluded that

$$\dot{\boldsymbol{e}}_{\eta}(t)=(\boldsymbol{A}-\boldsymbol{LC})\boldsymbol{e}_{\eta}(t)+\boldsymbol{B}\boldsymbol{e}_{\boldsymbol{\xi}}(t)+\varpi\boldsymbol{B}\boldsymbol{B}^{\mathrm{T}}\boldsymbol{e}_{\eta}(t)-\boldsymbol{L}\boldsymbol{v}(t) \tag{21}$$

$$\dot{\boldsymbol{e}}_{\xi}(t)=\dot{\boldsymbol{w}}(t)-\varpi\boldsymbol{B}^{\mathrm{T}}\left[\boldsymbol{A}\boldsymbol{e}_{\eta}(t)+\boldsymbol{B}\boldsymbol{e}_{\boldsymbol{\xi}}(t)+\varpi\boldsymbol{B}\boldsymbol{B}^{\mathrm{T}}\boldsymbol{e}_{\eta}(t)\right] \tag{22}$$

Denoting the aggregate state and disturbance as $\boldsymbol{\chi}(t)=\left[\boldsymbol{\eta}(t)^{\mathrm{T}}\quad \boldsymbol{e}_{\eta}(t)^{\mathrm{T}}\quad \boldsymbol{e}_{\xi}(t)^{\mathrm{T}}\right]^{\mathrm{T}}$ and $\boldsymbol{w}_{v}(t)=\left[\boldsymbol{v}(t)^{\mathrm{T}}\quad \dot{\boldsymbol{w}}(t)^{\mathrm{T}}\right]^{\mathrm{T}}$, one has

$$\dot{\boldsymbol{\chi}}(t)=\boldsymbol{A}_{\chi}\boldsymbol{\chi}(t)+\boldsymbol{B}_{\chi}\boldsymbol{w}_{v}(t) \tag{23}$$

where,

$$\boldsymbol{A}_{\chi}=\begin{bmatrix}\boldsymbol{A}-\boldsymbol{BK} & \boldsymbol{BK}+\varpi\boldsymbol{B}\boldsymbol{B}^{\mathrm{T}} & \boldsymbol{B}\\ 0 & \boldsymbol{A}-\boldsymbol{LC}+\varpi\boldsymbol{B}\boldsymbol{B}^{\mathrm{T}} & \boldsymbol{B}\\ 0 & -\varpi\boldsymbol{B}^{\mathrm{T}}\boldsymbol{A}-\varpi^{2}\boldsymbol{B}^{\mathrm{T}}\boldsymbol{B}\boldsymbol{B}^{\mathrm{T}} & -\varpi\boldsymbol{B}^{\mathrm{T}}\boldsymbol{B}\end{bmatrix},\boldsymbol{B}_{\chi}=\begin{bmatrix}0 & 0\\ -\boldsymbol{L} & 0\\ 0 & \boldsymbol{I}\end{bmatrix}$$

Remark 5: As a consequence of the fact that $\boldsymbol{w}(t)$ includes uncertain magnitudes, the initial estimation errors $\boldsymbol{e}_{\eta}(0)$ and $\boldsymbol{e}_{\xi}(0)$ are not easy to be exactly known, and the initial states of spacecraft may be unavailable, but they should be norm-bounded in practice. Then, for any symmetric positive definite matrix $\tilde{\boldsymbol{P}}_0$ of appropriate dimensions, there exist three positive scalars $\bar{\kappa}_k, k=1,2,3$ such that $\boldsymbol{\chi}_k(0)^{\mathrm{T}}\tilde{\boldsymbol{P}}_0\boldsymbol{\chi}_k(0)\le\bar{\kappa}_k^2\boldsymbol{1}_{1\times n}\tilde{\boldsymbol{P}}_0\boldsymbol{1}_{n\times 1}$, where $\boldsymbol{\chi}_1(0)=\boldsymbol{\eta}(0)$, $\boldsymbol{\chi}_2(0)=\boldsymbol{e}_{\eta}(0)$, $\boldsymbol{\chi}_3(0)=\boldsymbol{e}_{\xi}(0)$, $\boldsymbol{1}_{i\times j}$ denotes an *i* by *j* matrix (*i* rows, *j* columns) whose elements are all one, and n is the number of elements for $\boldsymbol{\chi}_k(0), k=1,2,3$.

Theorems 1 now gives the existence conditions of the controller gain matrix $\boldsymbol{K}$ and observer gain matrix $\boldsymbol{L}$.

Theorem 1 The closed-loop system represented by Eq. (23) is quadratically stable under controller (19), and $\boldsymbol{y}(t)$ satisfies an H_∞ performance constraint if there exist a positive scalar $\gamma_2=\gamma^2$, for given positive scalars ϖ, κ_3, $\bar{\kappa}_k>0, k=1,2,3$, given matrix $\boldsymbol{M}_0$, there exist symmetric positive definite matrices $\boldsymbol{X}_1,\boldsymbol{X}_3$ matrices $\boldsymbol{W}$ and $\boldsymbol{H}$, such that the following LMIs hold:

$$\begin{bmatrix}\boldsymbol{\Pi}_{11} & \boldsymbol{\Pi}_{12} & \boldsymbol{B}\boldsymbol{X}_3 & 0 & \boldsymbol{X}_1\boldsymbol{C}^{\mathrm{T}} & \boldsymbol{X}_1\boldsymbol{C}^{\mathrm{T}}\\ * & \boldsymbol{\Pi}_{22} & \boldsymbol{\Pi}_{23} & 0 & -\boldsymbol{X}_1\boldsymbol{M}_0 & 0\\ * & * & \boldsymbol{\Pi}_{33} & \boldsymbol{I} & 0 & 0\\ * & * & * & -\gamma_2\boldsymbol{I} & 0 & 0\\ * & * & * & * & (1-\gamma_2)\boldsymbol{I} & 0\\ * & * & * & * & * & -\boldsymbol{I}\end{bmatrix}<0 \tag{24}$$

$$\begin{bmatrix} -\alpha & \bar{\kappa}_1 \boldsymbol{1}_{1\times 6} & \bar{\kappa}_2 \boldsymbol{1}_{1\times 6} & \bar{\kappa}_3 \boldsymbol{1}_{1\times 3} \\ * & -\boldsymbol{X}_1 & 0 & 0 \\ * & * & -\boldsymbol{X}_1 & 0 \\ * & * & * & -\boldsymbol{X}_3 \end{bmatrix} < 0 \tag{25}$$

$$\begin{bmatrix} -k_0 \boldsymbol{X}_1 & 0 & 0 & 0 & \boldsymbol{W}^{\mathrm{T}} + \varpi \boldsymbol{X}_1 \boldsymbol{B} \\ * & -k_0 \boldsymbol{X}_1 & 0 & 0 & -\boldsymbol{W}^{\mathrm{T}} - \varpi \boldsymbol{X}_1 \boldsymbol{B} \\ * & * & -k_0 \boldsymbol{X}_3 & 0 & -\boldsymbol{X}_3 \\ * & * & * & -k_0 \kappa_3^{-2} \boldsymbol{I} & \boldsymbol{I} \\ * & * & * & * & -\boldsymbol{I} \end{bmatrix} < 0 \tag{26}$$

where,

$$\begin{aligned} \boldsymbol{\Pi}_{11} &= \boldsymbol{X}_1 \boldsymbol{A}^{\mathrm{T}} - \boldsymbol{W}^{\mathrm{T}} \boldsymbol{B}^{\mathrm{T}} + \boldsymbol{A}\boldsymbol{X}_1 - \boldsymbol{B}\boldsymbol{W} \\ \boldsymbol{\Pi}_{12} &= \boldsymbol{B}\boldsymbol{W} + \varpi \boldsymbol{B}\boldsymbol{B}^{\mathrm{T}} \boldsymbol{X}_1 \\ \boldsymbol{\Pi}_{22} &= \boldsymbol{X}_1 \boldsymbol{A}^{\mathrm{T}} - \boldsymbol{H}^{\mathrm{T}} + \boldsymbol{A}\boldsymbol{X}_1 - \boldsymbol{H} + \varpi \boldsymbol{B}\boldsymbol{B}^{\mathrm{T}} \boldsymbol{X}_1 + \varpi \boldsymbol{X}_1 \boldsymbol{B}\boldsymbol{B}^{\mathrm{T}} \\ \boldsymbol{\Pi}_{23} &= \boldsymbol{B}\boldsymbol{X}_3 - \varpi \boldsymbol{X}_1 \boldsymbol{A}^{\mathrm{T}} \boldsymbol{B} - \varpi^2 \boldsymbol{X}_1 \boldsymbol{B}\boldsymbol{B}^{\mathrm{T}} \boldsymbol{B} \\ \boldsymbol{\Pi}_{33} &= -\varpi (\boldsymbol{B}^{\mathrm{T}} \boldsymbol{B}\boldsymbol{X}_3 + \boldsymbol{X}_3 \boldsymbol{B}^{\mathrm{T}} \boldsymbol{B}) \end{aligned}$$

and $k_0 = (\alpha + 1)^{-1} \lambda^2$.

By minimizing γ_2, the optimal feasible solution of LMIs (24)-(26) is obtained, and one has the controller gain matrix $\boldsymbol{K} = \boldsymbol{W}\boldsymbol{X}_1^{-1}$ and the observer gain matrix $\boldsymbol{L} = \boldsymbol{H}\left(\boldsymbol{C}\boldsymbol{X}_1\right)^{-1}$.

Proof: First, it is shown that the closed-loop system (23) is quadratically stable while $\boldsymbol{v}(t) = 0, \dot{\boldsymbol{w}}(t) = 0$, and the definition of quadratic stability has been stated in [29].

Choose a Lyapunov function candidate as

$$V(t) = \boldsymbol{\eta}(t)^{\mathrm{T}} \boldsymbol{P}_1 \boldsymbol{\eta}(t) + \boldsymbol{e}_\eta(t)^{\mathrm{T}} \boldsymbol{P}_2 \boldsymbol{e}_\eta(t) + \boldsymbol{e}_\xi(t)^{\mathrm{T}} \boldsymbol{P}_3 \boldsymbol{e}_\xi(t) \tag{27}$$

satisfying $V(t) \le \alpha$, where $\boldsymbol{P}_1$, $\boldsymbol{P}_2$ and $\boldsymbol{P}_3$ are Lyapunov variables with $\boldsymbol{P}_1 = \boldsymbol{P}_2 = \boldsymbol{X}_1^{-1}, \boldsymbol{P}_3 = \boldsymbol{X}_3^{-1}$.

Before the next step of derivation, an assumption, i.e. $\boldsymbol{e}_\eta(t)^{\mathrm{T}} \boldsymbol{P}_2 \boldsymbol{L}\boldsymbol{v}(t) \ge \boldsymbol{e}_\eta(t)^{\mathrm{T}} \boldsymbol{M}_0 \boldsymbol{v}(t)$, is introduced first. As $\boldsymbol{e}_\eta(t), \boldsymbol{v}(t)$ are both bounded and $\boldsymbol{P}_2, \boldsymbol{L}$ are both fixed matrices before applications in aerospace engineering, the scalars $\boldsymbol{e}_\eta(t)^{\mathrm{T}} \boldsymbol{P}_2 \boldsymbol{L}\boldsymbol{v}(t)$ and $\boldsymbol{e}_\eta(t)^{\mathrm{T}} \boldsymbol{M}_0 \boldsymbol{v}(t)$ must be bounded, where $\boldsymbol{M}_0$ is a real matrix of appropriate dimension. As a result, $\boldsymbol{M}_0$ can be chosen appropriately such that the above assumption is established.

The time derivative of $V(t)$ along the system trajectories is given by

$$\dot{V}(t) = \dot{\boldsymbol{\eta}}(t)^{\mathrm{T}} \boldsymbol{P}_1 \boldsymbol{\eta}(t) + \boldsymbol{\eta}(t)^{\mathrm{T}} \boldsymbol{P}_1 \dot{\boldsymbol{\eta}}(t) + \dot{\boldsymbol{e}}_\eta(t)^{\mathrm{T}} \boldsymbol{P}_2 \boldsymbol{e}_\eta(t) + \boldsymbol{e}_\eta(t)^{\mathrm{T}} \boldsymbol{P}_2 \dot{\boldsymbol{e}}_\eta(t) + \dot{\boldsymbol{e}}_\xi(t)^{\mathrm{T}} \boldsymbol{P}_3 \boldsymbol{e}_\xi(t) + \boldsymbol{e}_\xi(t)^{\mathrm{T}} \boldsymbol{P}_3 \dot{\boldsymbol{e}}_\xi(t) \tag{28}$$

Now, substitution of Eqs. (20)-(22) into Eq. (27) leads to the following expression for $\dot{V}(t)$:

$$\begin{aligned}\dot{V}(t) &= \boldsymbol{\eta}(t)^{\mathrm{T}}\left[(\boldsymbol{A}-\boldsymbol{BK})^{\mathrm{T}}\boldsymbol{P}_1+\boldsymbol{P}_1(\boldsymbol{A}-\boldsymbol{BK})\right]\boldsymbol{\eta}(t)+2\boldsymbol{\eta}(t)^{\mathrm{T}}\boldsymbol{P}_1\boldsymbol{BK}\boldsymbol{e}_{\eta}(t)+2\boldsymbol{\eta}(t)^{\mathrm{T}}\boldsymbol{P}_1\boldsymbol{B}\boldsymbol{e}_{\boldsymbol{\xi}}(t)\\ &+2\varpi\boldsymbol{\eta}(t)^{\mathrm{T}}\boldsymbol{P}_1\boldsymbol{B}\boldsymbol{B}^{\mathrm{T}}\boldsymbol{e}_{\eta}(t)+\boldsymbol{e}_{\eta}(t)^{\mathrm{T}}\left[(\boldsymbol{A}-\boldsymbol{LC})^{\mathrm{T}}\boldsymbol{P}_2+\boldsymbol{P}_2(\boldsymbol{A}-\boldsymbol{LC})\right]\boldsymbol{e}_{\eta}(t)+2\boldsymbol{e}_{\eta}(t)^{\mathrm{T}}\boldsymbol{P}_2\boldsymbol{B}\boldsymbol{e}_{\xi}(t)\\ &+\boldsymbol{e}_{\eta}(t)^{\mathrm{T}}(\varpi\boldsymbol{P}_2\boldsymbol{B}\boldsymbol{B}^{\mathrm{T}}+\varpi\boldsymbol{B}\boldsymbol{B}^{\mathrm{T}}\boldsymbol{P}_2)\boldsymbol{e}_{\eta}(t)-2\boldsymbol{e}_{\eta}(t)^{\mathrm{T}}\boldsymbol{P}_2\boldsymbol{L}\boldsymbol{v}(t)+2\boldsymbol{e}_{\xi}(t)^{\mathrm{T}}\boldsymbol{P}_3\dot{\boldsymbol{w}}(t)\\ &-\varpi\boldsymbol{e}_{\xi}(t)^{\mathrm{T}}(\boldsymbol{P}_3\boldsymbol{B}^{\mathrm{T}}\boldsymbol{B}+\boldsymbol{B}^{\mathrm{T}}\boldsymbol{B}\boldsymbol{P}_3)\boldsymbol{e}_{\boldsymbol{\xi}}(t)-2\varpi\boldsymbol{e}_{\xi}(t)^{\mathrm{T}}\boldsymbol{P}_3\boldsymbol{B}^{\mathrm{T}}\left[\boldsymbol{A}\boldsymbol{e}_{\eta}(t)+\varpi\boldsymbol{B}\boldsymbol{B}^{\mathrm{T}}\boldsymbol{e}_{\eta}(t)\right]\end{aligned} \tag{29}$$

For $\boldsymbol{v}(t)=0,\dot{\boldsymbol{w}}(t)=0$, Eq.(29) reduces to

$$\begin{aligned}\dot{V}(t) &= \boldsymbol{\eta}(t)^{\mathrm{T}}\left[(\boldsymbol{A}-\boldsymbol{BK})^{\mathrm{T}}\boldsymbol{P}_1+\boldsymbol{P}_1(\boldsymbol{A}-\boldsymbol{BK})\right]\boldsymbol{\eta}(t)+2\boldsymbol{\eta}(t)^{\mathrm{T}}\boldsymbol{P}_1\boldsymbol{BK}\boldsymbol{e}_{\eta}(t)+2\boldsymbol{\eta}(t)^{\mathrm{T}}\boldsymbol{P}_1\boldsymbol{B}\boldsymbol{e}_{\boldsymbol{\xi}}(t)\\ &+2\varpi\boldsymbol{\eta}(t)^{\mathrm{T}}\boldsymbol{P}_1\boldsymbol{B}\boldsymbol{B}^{\mathrm{T}}\boldsymbol{e}_{\eta}(t)+\boldsymbol{e}_{\eta}(t)^{\mathrm{T}}\left[(\boldsymbol{A}-\boldsymbol{LC})^{\mathrm{T}}\boldsymbol{P}_2+\boldsymbol{P}_2(\boldsymbol{A}-\boldsymbol{LC})\right]\boldsymbol{e}_{\eta}(t)+2\boldsymbol{e}_{\eta}(t)^{\mathrm{T}}\boldsymbol{P}_2\boldsymbol{B}\boldsymbol{e}_{\xi}(t)\\ &+\boldsymbol{e}_{\eta}(t)^{\mathrm{T}}(\varpi\boldsymbol{P}_2\boldsymbol{B}\boldsymbol{B}^{\mathrm{T}}+\varpi\boldsymbol{B}\boldsymbol{B}^{\mathrm{T}}\boldsymbol{P}_2)\boldsymbol{e}_{\eta}(t)-\varpi\boldsymbol{e}_{\xi}(t)^{\mathrm{T}}(\boldsymbol{P}_3\boldsymbol{B}^{\mathrm{T}}\boldsymbol{B}+\boldsymbol{B}^{\mathrm{T}}\boldsymbol{B}\boldsymbol{P}_3)\boldsymbol{e}_{\boldsymbol{\xi}}(t)\\ &-2\varpi\boldsymbol{e}_{\xi}(t)^{\mathrm{T}}\boldsymbol{P}_3\boldsymbol{B}^{\mathrm{T}}\boldsymbol{A}\boldsymbol{e}_{\eta}(t)-2\varpi^2\boldsymbol{e}_{\xi}(t)^{\mathrm{T}}\boldsymbol{P}_3\boldsymbol{B}^{\mathrm{T}}\boldsymbol{B}\boldsymbol{B}^{\mathrm{T}}\boldsymbol{e}_{\eta}(t)\end{aligned} \tag{30}$$

Denote

$$\bar{\boldsymbol{\Theta}}_N=\begin{bmatrix}\bar{\boldsymbol{\Pi}}_{11} & \bar{\boldsymbol{\Pi}}_{12} & \boldsymbol{P}_1\boldsymbol{B}\\ * & \bar{\boldsymbol{\Pi}}_{22} & \bar{\boldsymbol{\Pi}}_{23}\\ * & * & \bar{\boldsymbol{\Pi}}_{33}\end{bmatrix}$$

where,

$$\begin{aligned}\bar{\boldsymbol{\Pi}}_{11} &= \boldsymbol{A}^{\mathrm{T}}\boldsymbol{P}_1-\boldsymbol{K}^{\mathrm{T}}\boldsymbol{B}^{\mathrm{T}}\boldsymbol{P}_1+\boldsymbol{P}_1\boldsymbol{A}-\boldsymbol{P}_1\boldsymbol{BK}\\ \bar{\boldsymbol{\Pi}}_{12} &= \boldsymbol{P}_1\boldsymbol{BK}+\varpi\boldsymbol{P}_1\boldsymbol{B}\boldsymbol{B}^{\mathrm{T}}\\ \bar{\boldsymbol{\Pi}}_{22} &= \boldsymbol{A}^{\mathrm{T}}\boldsymbol{P}_2-\boldsymbol{C}^{\mathrm{T}}\boldsymbol{L}^{\mathrm{T}}\boldsymbol{P}_2+\boldsymbol{P}_2\boldsymbol{A}-\boldsymbol{P}_2\boldsymbol{LC}+\varpi\boldsymbol{P}_2\boldsymbol{B}\boldsymbol{B}^{\mathrm{T}}+\varpi\boldsymbol{B}\boldsymbol{B}^{\mathrm{T}}\boldsymbol{P}_2\\ \bar{\boldsymbol{\Pi}}_{23} &= \boldsymbol{P}_2\boldsymbol{B}-\varpi\boldsymbol{A}^{\mathrm{T}}\boldsymbol{B}\boldsymbol{P}_3-\varpi^2\boldsymbol{B}\boldsymbol{B}^{\mathrm{T}}\boldsymbol{B}\boldsymbol{P}_3\\ \bar{\boldsymbol{\Pi}}_{33} &= -\varpi(\boldsymbol{P}_3\boldsymbol{B}^{\mathrm{T}}\boldsymbol{B}+\boldsymbol{B}^{\mathrm{T}}\boldsymbol{B}\boldsymbol{P}_3)\end{aligned}$$

The first derivative of the Lyapunov function becomes

$$\dot{V}(t)=\boldsymbol{\chi}(t)^{\mathrm{T}}\bar{\boldsymbol{\Theta}}_N\boldsymbol{\chi}(t)$$

Considering inequality (24), multiplied by $\mathrm{diag}\left\{\begin{bmatrix}\boldsymbol{P}_1 & \boldsymbol{P}_2 & \boldsymbol{P}_3 & \boldsymbol{I} & \boldsymbol{I} & \boldsymbol{I}\end{bmatrix}\right\}$ at both sides simultaneously, one has

$$\begin{bmatrix}\bar{\boldsymbol{\Pi}}_{11} & \bar{\boldsymbol{\Pi}}_{12} & \boldsymbol{P}_1\boldsymbol{B} & 0 & \boldsymbol{C}^{\mathrm{T}} & \boldsymbol{C}^{\mathrm{T}}\\ * & \bar{\boldsymbol{\Pi}}_{22} & \bar{\boldsymbol{\Pi}}_{23} & 0 & -\boldsymbol{M}_0 & 0\\ * & * & \bar{\boldsymbol{\Pi}}_{33} & \boldsymbol{P}_3 & 0 & 0\\ * & * & * & -\gamma_2\boldsymbol{I} & 0 & 0\\ * & * & * & * & (1-\gamma_2)\boldsymbol{I} & 0\\ * & * & * & * & * & -\boldsymbol{I}\end{bmatrix}<0 \tag{31}$$

According to inequality (31) and Lemma 1, one has $\bar{\boldsymbol{\Theta}}_N<0$, so that

$$\dot{V}(t) = \boldsymbol{\chi}(t)^{\mathrm{T}} \bar{\boldsymbol{\Theta}}_N \boldsymbol{\chi}(t) \le \lambda_{\max}(\bar{\boldsymbol{\Theta}}_N) \|\boldsymbol{\chi}\|^2$$

Furthermore, let $\bar{\alpha} = -\lambda_{\max}(\bar{\boldsymbol{\Theta}}_N) > 0$, then,

$$\dot{V}(t) \le -\bar{\alpha} \|\boldsymbol{\chi}\|^2 \tag{32}$$

i.e., the closed-loop system (23) is quadratically stable under controller (19) .

Next, it is shown that the output $\boldsymbol{y}(t)$ satisfies an H_∞ performance constraint.

To establish the $L_2[0, \infty)$ norm bound $\gamma^2 \|\tilde{\boldsymbol{w}}(t)\|_2^2$, where $\tilde{\boldsymbol{w}}(t)$ is a constructed vector with norm $\|\tilde{\boldsymbol{w}}\| = \sqrt{\dot{\boldsymbol{w}}^2 + \boldsymbol{v}^2}$, consider the following functional:

$$J = \int_0^{+\infty} [\boldsymbol{y}(t)^{\mathrm{T}} \boldsymbol{y}(t) - \gamma^2 \tilde{\boldsymbol{w}}(t)^{\mathrm{T}} \tilde{\boldsymbol{w}}(t)] dt$$

As the closed-loop system has quadratic stability, for arbitrary nonzero $\tilde{\boldsymbol{w}}(t) \in L_2[0,\infty)$, under zero initial conditions, one has

$$\begin{aligned}
J &= \int_0^{+\infty} [\boldsymbol{y}(t)^{\mathrm{T}} \boldsymbol{y}(t) - \gamma^2 \tilde{\boldsymbol{w}}(t)^{\mathrm{T}} \tilde{\boldsymbol{w}}(t) + \dot{V}(t)] dt - V(\infty) + V(0) \\
&\le \int_0^{+\infty} \begin{Bmatrix} \boldsymbol{\eta}(t)^{\mathrm{T}} \boldsymbol{C}^{\mathrm{T}} \boldsymbol{C} \boldsymbol{\eta}(t) + 2\boldsymbol{\eta}(t)^{\mathrm{T}} \boldsymbol{C}^{\mathrm{T}} \boldsymbol{v}(t) + \boldsymbol{v}(t)^{\mathrm{T}} \boldsymbol{v}(t) \\ -\gamma^2 \left[\dot{\boldsymbol{w}}(t)^{\mathrm{T}} \dot{\boldsymbol{w}}(t) + \boldsymbol{v}(t)^{\mathrm{T}} \boldsymbol{v}(t) \right] + \boldsymbol{\chi}(t)^{\mathrm{T}} \bar{\boldsymbol{\Theta}}_N \boldsymbol{\chi}(t) \\ -2\boldsymbol{e}_\eta(t)^{\mathrm{T}} \boldsymbol{P}_2 \boldsymbol{L} \boldsymbol{v}(t) + 2\boldsymbol{e}_\xi(t)^{\mathrm{T}} \boldsymbol{P}_3 \dot{\boldsymbol{w}}(t) \end{Bmatrix} dt \\
&\le \int_0^{+\infty} \begin{bmatrix} \boldsymbol{\eta}(t)^{\mathrm{T}} & \boldsymbol{e}_\eta(t)^{\mathrm{T}} & \boldsymbol{e}_\xi(t)^{\mathrm{T}} & \dot{\boldsymbol{w}}(t)^{\mathrm{T}} & \boldsymbol{v}(t)^{\mathrm{T}} \end{bmatrix} \begin{bmatrix} \bar{\boldsymbol{\Pi}}_{11} + \boldsymbol{C}^{\mathrm{T}} \boldsymbol{C} & \bar{\boldsymbol{\Pi}}_{12} & \boldsymbol{P}_1 \boldsymbol{B} & 0 & \boldsymbol{C}^{\mathrm{T}} \\ * & \bar{\boldsymbol{\Pi}}_{22} & \bar{\boldsymbol{\Pi}}_{23} & 0 & -\boldsymbol{M}_0 \\ * & * & \bar{\boldsymbol{\Pi}}_{33} & \boldsymbol{P}_3 & 0 \\ * & * & * & -\gamma^2 \boldsymbol{I} & 0 \\ * & * & * & * & (1-\gamma^2)\boldsymbol{I} \end{bmatrix} \begin{bmatrix} \boldsymbol{\eta}(t) \\ \boldsymbol{e}_\eta(t) \\ \boldsymbol{e}_\xi(t) \\ \dot{\boldsymbol{w}}(t) \\ \boldsymbol{v}(t) \end{bmatrix} dt
\end{aligned}$$

According to Lemma 1 and inequality (31), $J < 0$ holds, i.e. $\boldsymbol{z}$(t) satisfies an H_∞ performance constraint.

Finally, it is shown that the control input is constrained, i.e., it satisfies the condition of inequality (10).

According to Lemma 1, the inequality (25) is equivalent to

$$\bar{\kappa}_1^2 \boldsymbol{1}_{1\times 6} \boldsymbol{P}_1 \boldsymbol{1}_{6\times 1} + \bar{\kappa}_2^2 \boldsymbol{1}_{1\times 6} \boldsymbol{P}_2 \boldsymbol{1}_{6\times 1} + \bar{\kappa}_3^2 \boldsymbol{1}_{1\times 3} \boldsymbol{P}_3 \boldsymbol{1}_{3\times 1} < \alpha \tag{33}$$

Due to the fact pointed out in Remark 5, it is easily obtained that

$$\boldsymbol{\eta}(0)^{\mathrm{T}} \boldsymbol{P}_1 \boldsymbol{\eta}(0) + \boldsymbol{e}_\eta(0)^{\mathrm{T}} \boldsymbol{P}_2 \boldsymbol{e}_\eta(0) + \boldsymbol{e}_\xi(0)^{\mathrm{T}} \boldsymbol{P}_3 \boldsymbol{e}_\xi(0) < \alpha \tag{34}$$

Considering inequality(26), multiplied by $\mathrm{diag}\{[\boldsymbol{P}_1 \quad \boldsymbol{P}_2 \quad \boldsymbol{P}_3 \quad \boldsymbol{I} \quad \boldsymbol{I}]\}$ at both sides simultaneously, one has

$$\begin{bmatrix} -k_0\boldsymbol{P}_1 & 0 & 0 & 0 & \boldsymbol{K}^{\mathrm{T}}+\varpi\boldsymbol{B} \\ * & -k_0\boldsymbol{P}_2 & 0 & 0 & -\boldsymbol{K}^{\mathrm{T}}-\varpi\boldsymbol{B} \\ * & * & -k_0\boldsymbol{P}_3 & 0 & -\boldsymbol{I} \\ * & * & * & -k_0\kappa_3^{-2}\boldsymbol{I} & \boldsymbol{I} \\ * & * & * & * & -\boldsymbol{I} \end{bmatrix} < 0 \tag{35}$$

Using Lemma 1, one has

$$\begin{bmatrix} (\boldsymbol{K}+\varpi\boldsymbol{B}^{\mathrm{T}})^{\mathrm{T}} \\ -(\boldsymbol{K}+\varpi\boldsymbol{B}^{\mathrm{T}})^{\mathrm{T}} \\ -\boldsymbol{I} \\ \boldsymbol{I} \end{bmatrix} \begin{bmatrix} \boldsymbol{K}+\varpi\boldsymbol{B}^{\mathrm{T}} & -(\boldsymbol{K}+\varpi\boldsymbol{B}^{\mathrm{T}}) & -\boldsymbol{I} & \boldsymbol{I} \end{bmatrix} < \begin{bmatrix} k_0\boldsymbol{P}_1 & 0 & 0 & 0 \\ * & k_0\boldsymbol{P}_2 & 0 & 0 \\ * & * & k_0\boldsymbol{P}_3 & 0 \\ * & * & * & k_0\kappa_3^{-2}\boldsymbol{I} \end{bmatrix} \tag{36}$$

According to Eq. (19), one has

$$\begin{aligned} \left\|\boldsymbol{u}(t)\right\|_2^2 &= \boldsymbol{u}(t)^{\mathrm{T}}\boldsymbol{u}(t) \\ &= \left[-\boldsymbol{K}\hat{\boldsymbol{\eta}}(t)-\hat{\boldsymbol{w}}(t)\right]^{\mathrm{T}}\left[-\boldsymbol{K}\hat{\boldsymbol{\eta}}(t)-\hat{\boldsymbol{w}}(t)\right] \\ &= \left[\boldsymbol{K}\left(\boldsymbol{\eta}(t)-\boldsymbol{e}_\eta(t)\right)+\boldsymbol{\xi}(t)-\boldsymbol{e}_\xi(t)+\varpi\boldsymbol{B}^{\mathrm{T}}\left(\boldsymbol{\eta}(t)-\boldsymbol{e}_\eta(t)\right)\right]^{\mathrm{T}}\left[\boldsymbol{K}\left(\boldsymbol{\eta}(t)-\boldsymbol{e}_\eta(t)\right)+\boldsymbol{\xi}(t)-\boldsymbol{e}_\xi(t)+\varpi\boldsymbol{B}^{\mathrm{T}}\left(\boldsymbol{\eta}(t)-\boldsymbol{e}_\eta(t)\right)\right] \\ &= \begin{bmatrix} \boldsymbol{\eta}(t)^{\mathrm{T}} & \boldsymbol{e}_\eta(t)^{\mathrm{T}} & \boldsymbol{e}_\xi(t)^{\mathrm{T}} & \boldsymbol{\xi}(t)^{\mathrm{T}} \end{bmatrix} \begin{bmatrix} (\boldsymbol{K}+\varpi\boldsymbol{B}^{\mathrm{T}})^{\mathrm{T}} \\ -(\boldsymbol{K}+\varpi\boldsymbol{B}^{\mathrm{T}})^{\mathrm{T}} \\ -\boldsymbol{I} \\ \boldsymbol{I} \end{bmatrix} \begin{bmatrix} \boldsymbol{K}+\varpi\boldsymbol{B}^{\mathrm{T}} & -(\boldsymbol{K}+\varpi\boldsymbol{B}^{\mathrm{T}}) & -\boldsymbol{I} & \boldsymbol{I} \end{bmatrix} \begin{bmatrix} \boldsymbol{\eta}(t) \\ \boldsymbol{e}_\eta(t) \\ \boldsymbol{e}_\xi(t) \\ \boldsymbol{\xi}(t) \end{bmatrix} \\ &< \begin{bmatrix} \boldsymbol{\eta}(t)^{\mathrm{T}} & \boldsymbol{e}_\eta(t)^{\mathrm{T}} & \boldsymbol{e}_\xi(t)^{\mathrm{T}} & \boldsymbol{\xi}(t)^{\mathrm{T}} \end{bmatrix} \begin{bmatrix} k_0\boldsymbol{P}_1 & 0 & 0 & 0 \\ * & k_0\boldsymbol{P}_2 & 0 & 0 \\ * & * & k_0\boldsymbol{P}_3 & 0 \\ * & * & * & k_0\kappa_3^{-2}\boldsymbol{I} \end{bmatrix} \begin{bmatrix} \boldsymbol{\eta}(t) \\ \boldsymbol{e}_\eta(t) \\ \boldsymbol{e}_\xi(t) \\ \boldsymbol{\xi}(t) \end{bmatrix} \\ &= k_0\left(\boldsymbol{\eta}(t)^{\mathrm{T}}\boldsymbol{P}_1\boldsymbol{\eta}(t)+\boldsymbol{e}_\eta(t)^{\mathrm{T}}\boldsymbol{P}_2\boldsymbol{e}_\eta(t)+\boldsymbol{e}_\xi(t)^{\mathrm{T}}\boldsymbol{P}_3\boldsymbol{e}_\xi(t)+\kappa_3^{-2}\boldsymbol{\xi}(t)^{\mathrm{T}}\boldsymbol{\xi}(t)\right) \\ &\le k_0\left(V(t)+1\right) \end{aligned}$$

According to inequalities (32) and (34), one knows

$$\left\|\boldsymbol{u}(t)\right\|_2^2 < k_0\left(\alpha+1\right) = \lambda^2 \tag{37}$$

This completes the proof.

4. Simulation Results

In this section, the effectiveness of the intermediate observer-based controller is illustrated with simulations of a spacecraft electromagnetic docking system. In this example, for 'CM' orbit, the eccentricity e=0.15, the semi-major axis a=10000km, the initial true anomaly $\theta(0)$=0, and m_0 is only representative of a valid mass with value of 20kg. Whatever the initial guess of m_0, the difference compared with the true value of m_{CT} can be attributed to the matrix

uncertainty $\Delta \boldsymbol{B}$ or even the lumped disturbance, and the lumped disturbance can be estimated for the anti-disturbance controller design. The unknown mass of the chaser and target spacecraft are assumed to be $m_{\mathrm{C}} = 40\mathrm{kg}$ and $m_{\mathrm{T}} = 100\,\mathrm{kg}$, respectively. Choose the initial states as $\boldsymbol{\eta}(0)$=[2m, 3m, 4m, 0m/s, 0m/s, 0m/s]$^{\mathrm{T}}$, $\boldsymbol{e}(0)$=[0N, 0N, 0N]$^{\mathrm{T}}$, the gravitational parameter μ=3.986×10^{5}km^3/s^2, and the permeability of free space $\mu_0 = 4\pi \times 10^{-7}\,\mathrm{N \cdot A^{-2}}$; the magnetic moment of target spacecraft is assumed to be $\boldsymbol{\mu}_{\mathrm{T}} = \left[-2.29 \quad -8.17 \quad -2.33\right]^{\mathrm{T}} \times 10^5\,\mathrm{Am}^2$, and the control force is constrained by λ= 30N. Here, an actuator additive fault is assumed to occur, i.e. $\boldsymbol{E}$=$\boldsymbol{B}$, with the fault signals $\boldsymbol{f}(t) = [8\ 9\ 4]^{\mathrm{T}} \times 10^{-2}\,\overline{f}(t)$, and the form of $\overline{f}(t)$ is shown in Table 1.

Table 1. The form of $\overline{f}(t)$

t/s	[0,2]	(2, 5]	(5,10]	(10,13]	(13,15]
$\overline{f}(t)$/ N	0	sin(0.1πt)	1	cos(0.1πt)	0

For comparative purposes, two cases are studied in this section. In the first case, the proposed intermediate observer-based controller (IOBC) is applied for spacecraft electromagnetic docking. In the second case, the disturbance observer-based controller (DOBC) introduced in [8] is employed, wherein comparison results are given to illustrate the advantages of the approach proposed in this paper. All simulation parameters are identical in these two cases. In both cases, the maximum of control force on each channel is set to be 17.321N, so that the norm maximum of control force is 30N.

In addition, to compare the control performance of IOBC and DOBC precisely, the measurement errors and external disturbances are also chosen according to [8]. Then the measurement errors are assumed to be $\boldsymbol{v}(t) = 10^{-4} \times \left[4 \quad 5 \quad 6 \quad 0.2 \quad 0.2 \quad 0.2\right]^{\mathrm{T}} \sin(0.01\pi t)$. The environmental disturbance has been analyzed in [30] in detail, which includes gravity-gradient force, aerodynamic force, and the force of Earth magnetic field. As pointed out in this work, the sinusoid is the prototype of periodic disturbances, and the environmental disturbance force such as magnetic force and gravity-gradient force are cyclic essentially which can be represented by sinusoids. Combined with aerodynamic force, the external disturbance force can contain constant term. Thus, the external disturbances for the chaser and target spacecraft used in the simulation are taken to be of the following form:

$$\boldsymbol{w}_{\mathrm{C}}(t)=\begin{bmatrix}0.1+0.2\sin(0.11\pi t)\\0.15+0.2\cos(0.11\pi t)\\0.2+0.3\cos(0.11\pi t+\pi/3)\end{bmatrix}\mathrm{N},$$

$$\boldsymbol{w}_{\mathrm{T}}(t)=\begin{bmatrix}0.1+0.1\sin(0.11\pi t)\\0.2+0.12\cos(0.11\pi t+\pi/4)\\0.3+0.15\cos(0.11\pi t+\pi/6)\end{bmatrix}\mathrm{N}$$

Meanwhile, choose $\varpi=200,\kappa_3=10,\overline{\kappa}_1=4.0012,\overline{\kappa}_2=4.0012,\overline{\kappa}_3=0.032,\lambda=30,\alpha=7999$, then one has $k_0=0.1125$.

In addition, $\boldsymbol{M}_0$ is chosen as

$$\boldsymbol{M}_0=\begin{bmatrix}3.5321&0&-0.0003&1.8781&0&-0.0003\\0&3.5321&0&0&1.8781&0\\0.0003&0&3.5321&0.0003&0&1.8781\\1.8895&0&0.0003&4.1465&0&0.0002\\0&1.8895&0&0&4.1465&0\\-0.0003&0&1.8895&-0.0002&0&4.1465\end{bmatrix}$$

A. Intermediate observer-based controller

Solving LMIs (24)-(26) gives

$$\boldsymbol{X}_1=\begin{bmatrix}0.0084&0&-0.0000&-0.0033&0&0.0000\\0&0.0084&0&0&-0.0033&0\\-0.0000&0&0.0084&-0.0000&0&-0.0033\\-0.0033&0&-0.0000&0.0100&0&-0.0000\\0&-0.0033&0&0&0.0100&0\\0.0000&0&-0.0033&-0.0000&0&0.0100\end{bmatrix}$$

$$\boldsymbol{X}_3=\begin{bmatrix}1.5547&0&-0.0000\\0&1.5547&0\\-0.0000&0&1.5547\end{bmatrix}$$

$$\boldsymbol{W}=\begin{bmatrix}0.1293&0&-0.0001&0.3067&0&0.0003\\0&0.1293&0&0&0.3067&0\\0.0001&0&0.1293&-0.0003&0&0.3067\end{bmatrix}$$

$$\boldsymbol{H}=\begin{bmatrix}0.0236&0&-0.0000&0.0023&0&0.0000\\0&0.0236&0&0&0.0023&0\\0.0000&0&0.0236&-0.0000&0&0.0023\\0.0074&0&0.0000&0.0354&0&0.0000\\0&0.0074&0&0&0.0354&0\\-0.0000&0&0.0074&-0.0000&0&0.0354\end{bmatrix}$$

Then, the controller gain matrix and the intermediate observer gain matrix are obtained as follows:

$$\boldsymbol{K} = \boldsymbol{W}\boldsymbol{X}_1^{-1} = \begin{bmatrix} 31.1662 & 0 & 0.0028 & 40.7582 & 0 & 0.0252 \\ 0 & 31.1661 & 0 & 0 & 40.7581 & 0 \\ -0.0028 & 0 & 31.1662 & -0.0252 & 0 & 40.7582 \end{bmatrix}$$

$$\boldsymbol{L} = \boldsymbol{H}(\boldsymbol{C}\boldsymbol{X}_1)^{-1} = \begin{bmatrix} 3.3049 & 0 & -0.0001 & 1.3034 & 0 & -0.0003 \\ 0 & 3.3049 & 0 & 0 & 1.3034 & 0 \\ 0.0001 & 0 & 3.3049 & 0.0003 & 0 & 1.3034 \\ 2.5759 & 0 & 0.0005 & 4.3737 & 0 & 0.0000 \\ 0 & 2.5759 & 0 & 0 & 4.3737 & 0 \\ -0.0005 & 0 & 2.5759 & -0.0000 & 0 & 4.3737 \end{bmatrix}$$

Applying the controller gain $\boldsymbol{K}$ and observer gain $\boldsymbol{L}$ to the closed-loop electromagnetic docking system expressed by Eq.(23) produces the simulation results of Figs.2-9. As shown in Figs.2 and 3, the relative position and velocity asymptotically converge to a small bound containing zero with steady-state errors less than 7×10^{-3} m and 4×10^{-3} m/s respectively, thus can be safely neglected. In addition, the relative velocity satisfies the requirement of soft docking. Figs. 4-5 plot the estimation errors of relative position and velocity, which suggest that they are successfully estimated within 2s and 6s respectively. It can be concluded that the intermediate observer developed in this paper can effectively estimate the relative motion information, with a fast convergence speed. The sphere with a radius of 0.12 N in Fig.6 means that the estimation error of lumped disturbance will converge to a small neighborhood containing equilibrium. The blue curve denotes estimation error out of the neighborhood while the red curve represents when the estimation error arrives in the convergence set, it will be attracted and stay in the sphere. The magnitude of control force is plotted in Fig. 7, from which one can see that the magnitude of control force along each axis is less than 17.321N. It is obvious that the 2-norm of control force is less than 30N, which satisfies the prescribed limitations. It is noted that the proposed scheme in this paper can achieve spacecraft electromagnetic docking mission in elliptical orbit with high accuracy and very good performance in the presence of external disturbances, fault signals, unknown mass, elliptical eccentricity, measurement errors and input constraints. Thus, the simulation results verify the theoretical analysis and demonstrate the effectiveness of the presented control strategy based on intermediate observer.

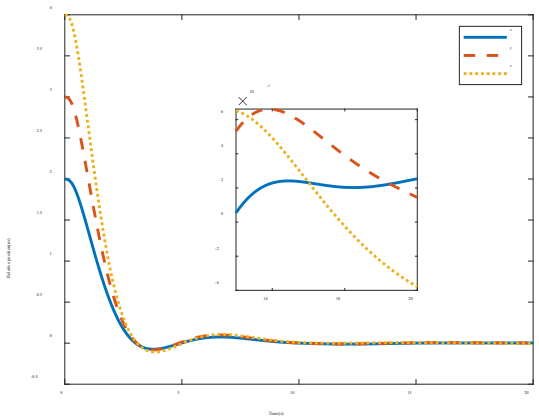

Fig. 2 Time response of relative position

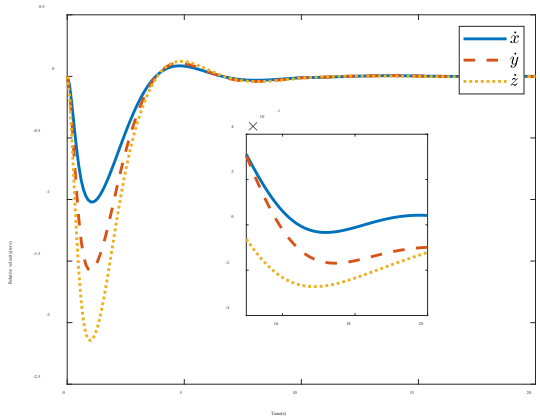

Fig. 3 Time response of relative velocity

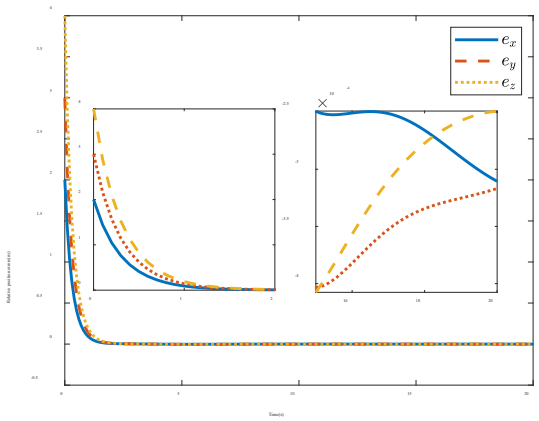

Fig. 4 Estimation errors of relative position

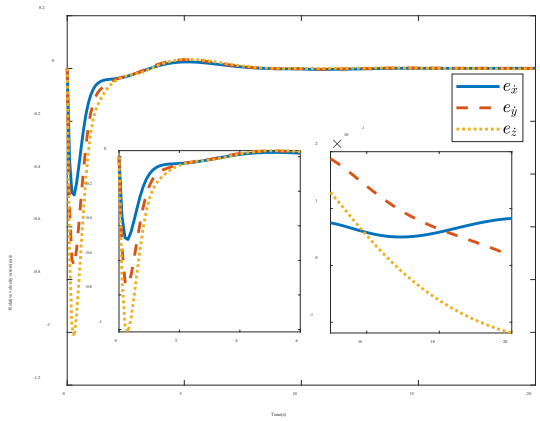

Fig. 5 Estimation errors of relative velocity

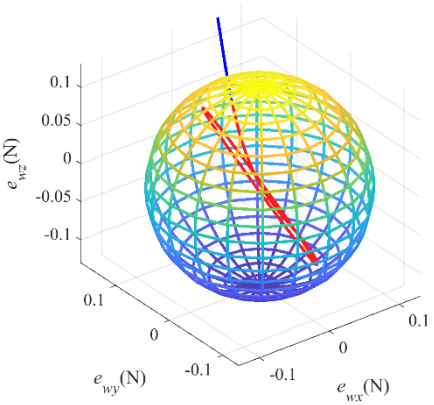

Fig. 6 The convergence set of disturbance estimation errors

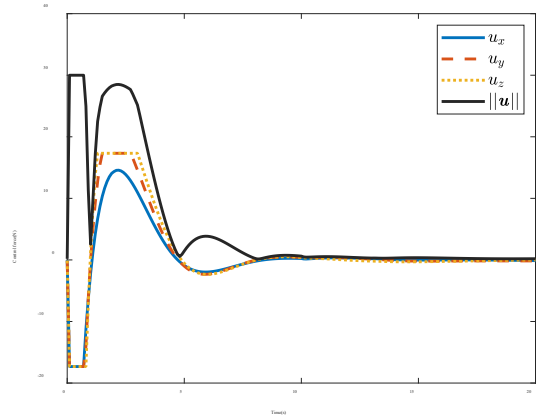

Fig. 7 Time response of control force

To further illustrate the motion of chaser and target spacecraft relative to 'CM', Fig.8 is presented, wherein the color-bar represents the simulation time. As one can see, the chaser spacecraft occupies a longer relative motion distance than the target spacecraft. This is because the mass of target spacecraft is larger than the chaser spacecraft, which leads to the fact that 'CM' is closer to the center of mass of target spacecraft. Fig.9 depicts the solved magnetic moment of the chaser spacecraft based on Eq.(8), from which one can see that the maximum of magnetic moment is less than $7\times10^4\mathrm{Am}^2$, which is practical and can be provided by a common electromagnetic mechanism.

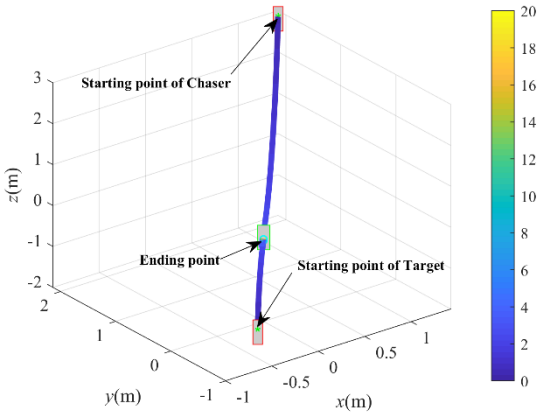

Fig. 8 Motion of chaser and target spacecraft relative to 'CM' in three-dimensional visualization

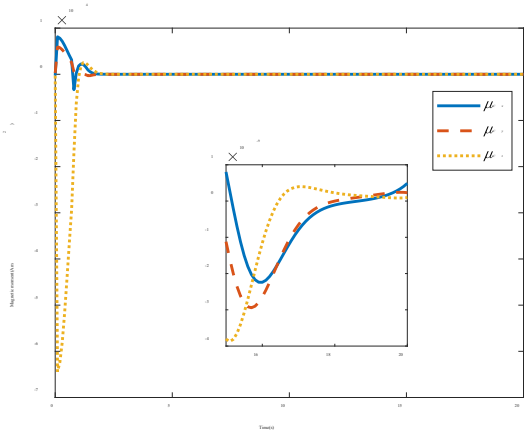

Fig. 9 Magnetic moment of chaser spacecraft

B. Disturbance observer-based controller

In this case, the controller gain matrix $\boldsymbol{K}$ and disturbance observer gain matrix are as follows:

$$\boldsymbol{K}=\begin{bmatrix} 0.4385 & -0.0024 & -0.0060 & 4.5770 & -0.0113 & -0.0151 \\ -0.0024 & 0.4366 & -0.0047 & -0.0114 & 4.5670 & -0.0233 \\ -0.0003 & -0.0047 & 0.4338 & -0.0153 & -0.0234 & 4.5532 \end{bmatrix}$$

$$\boldsymbol{L}=\begin{bmatrix} 0 & 0 & 0 & 2519.2 & 0.0753 & 0.1004 \\ 0 & 0 & 0 & 0.0753 & 2519.3 & 0.1508 \\ 0 & 0 & 0 & 0.1004 & 0.1508 & 2519.4 \end{bmatrix}$$

Applying this controller to the corresponding electromagnetic docking system represented by Eq.(23) produces the simulation results of Figs. 10-13. Figs. 10 and 11 plot the response curves of relative position and relative velocity between the two spacecraft, from which it can be seen that the DOBC can achieve electromagnetic docking within 30s while the IOBC stabilizes the system with better performance -within only 15s. Fig. 12 depicts the comparison results

of control force norm between the IOBC and DOBC schemes, which suggests that the maximum control force norm for DOBC is approximately 3.5N, much smaller than the electromagnetic force limit - 30N that can be provided. To further illustrate the advantage of the IOBC scheme proposed in this paper, comparison results are given from the perspective of control force utilization efficiency, see Fig. 13. It is noted that the control force utilization efficiency is defined by $\Upsilon=\int_0^T\left(\|\boldsymbol{u}\|/\lambda\right)\mathrm{d}t$, where T denotes the simulation time, and T = 60s is chosen in the simulation. It is observed that the proposed IOBC has higher force utilization efficiency - approximately 6.5% than the DOBC - less than 1%, i.e., the DOBC does not make effective use of the control force that the actuator can provide, leading to much slower speed of convergence. More importantly, the IOBC doesn't require the prior information on relative motion information while the DOBC does. It can be concluded that according to the measures used here, the proposed IOBC in this paper is superior to the DOBC from the perspective of convergence time and control force utilization efficiency.

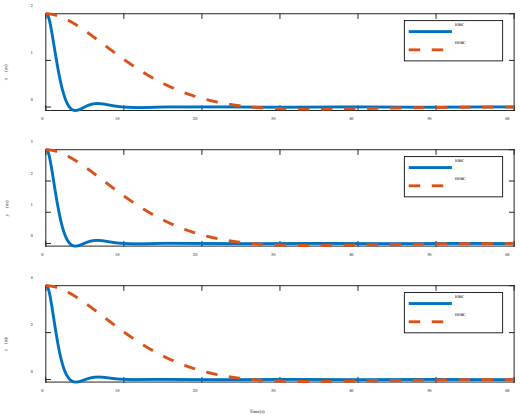

Fig. 10 Comparison results of relative position

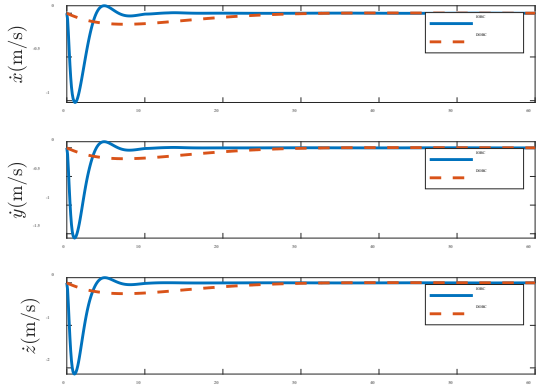

Fig. 11 Comparison results of relative velocity

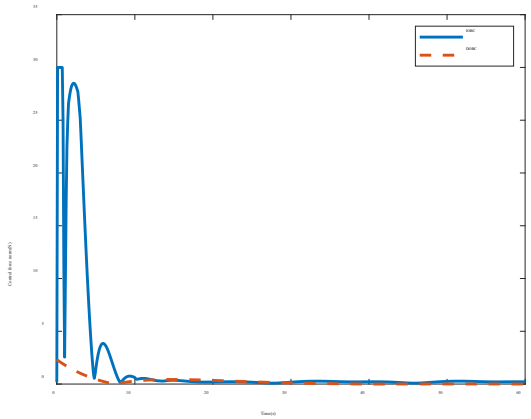

Fig. 12 Comparison results of control force norm

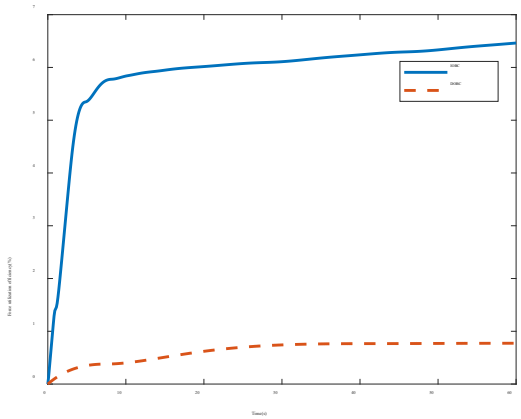

Fig. 13 Comparison results of control force utilization efficiency

5. Conclusions

This paper presents a novel intermediate observer-based control strategy for spacecraft electromagnetic docking in the presence of external disturbances, fault signals, unknown mass, elliptical eccentricity, measurement errors and input constraints. By analyzing the effects of multiple uncertain factors, a lumped disturbance is constructed to facilitate controller design. Then, a new auxiliary variable constituted of relative motion information and the lumped disturbance is introduced for the design of the intermediate observer. Based on this, a feedback control law employing the estimates of relative motion information and the lumped disturbance is developed. Furthermore, the sufficient condition for input constraints can also be incorporated into the controller design, to satisfy the actuator constraints. It is worth noting that the developed controller requires no information on the mass of chaser and target spacecraft, external disturbances and fault signals. Simulation results illustrate the effectiveness and feasibility of the developed intermediate observer-based controller, which also demonstrate that the relative motion information can be estimated effectively. The performance of the proposed intermediate observer-based controller is also compared with disturbance observer-based controller over several dense and complex 2D and 3D simulation scenarios, with results outperforming existing methods.

Acknowledgements

This work is supported by the Fundamental Research Funds for the Central Universities (3102019HTQD007) and National Natural Science Foundation of China (11972026).

Declaration of competing interest

None declared.

References

[1] Ahsun U, Miller D W, Ramirez-Riberos J L. Control of electromagnetic satellite formations in near-earth orbits. Journal of guidance, control, and dynamics, 2010, 33(6): 1883-1891.

[2] Zhang Y, Yang L, Zhu Y, et al. Angular-Momentum Management of Spacecraft Electromagnetic Docking Considering the Earth's Magnetic Field. Journal of Guidance, Control, and Dynamics, 2013, 36(3): 860-869.

[3] Zhang Y, Yang L, Zhu Y, et al. Nonlinear 6-DOF control of spacecraft docking with inter-satellite electromagnetic force. Acta Astronautica, 2012, 77: 97-108.

[4] Norman M C, Peck M A. Stationkeeping of a flux-pinned satellite network. Journal of guidance, control, and dynamics, 2010, 33(5): 1683-1687.

[5] Zhu Y, Cai W, Yang L, et al. Flatness-based trajectory planning for electromagnetic spacecraft proximity operations in elliptical orbits. Acta Astronautica, 2018, 152: 342-351.

[6] Kong EM. Spacecraft formation flight exploiting potential fields. Ph.D. Thesis, Massachusetts Institute of Technology, February 2002: 145-146.

[7] Elias L M, Kwon D W, Sedwick R J, et al. Electromagnetic formation flight dynamics including reaction wheel gyroscopic stiffening effects. Journal of Guidance, Control, and Dynamics, 2007, 30(2): 499-511.

[8] Shi K, Liu C, Sun Z. Constrained fuel-free control for spacecraft electromagnetic docking in elliptical orbits. Acta Astronautica, 2019, 162: 14-24.

[9] Liu C, Vukovich G, Shi K, Sun Z. Robust fault tolerant nonfragile H_∞ attitude control for spacecraft via stochastically intermediate observer. Advances in Space Research, 2018, 62(9): 2631-2648.

[10] Narula A, Biggs J D. Fault-tolerant station-keeping on libration point orbits. Journal of Guidance, Control, and Dynamics, 2017, 41(4): 879-887.

[11] Sanyal A, Fosbury A, Chaturvedi N, et al. Inertia-free spacecraft attitude tracking with disturbance rejection and almost global stabilization. Journal of guidance, control, and dynamics, 2009, 32(4): 1167-1178.

[12] Liu C, Yue X, Shi K, et al. Inertia-free attitude stabilization for flexible spacecraft with active vibration suppression. International Journal of Robust and Nonlinear Control, 2019, 29(18): 6311-6336.

[13] Singla P, Subbarao K, Junkins J L. Adaptive output feedback control for spacecraft rendezvous and docking under measurement uncertainty. Journal of guidance, control, and dynamics, 2006, 29(4): 892-902.

[14] Sun L, Zheng Z. Saturated adaptive hierarchical fuzzy attitude-tracking control of rigid spacecraft with modeling and measurement uncertainties. IEEE Transactions on Industrial Electronics, 2018, 66(5): 3742-3751.

[15] Chen WH, Yang J, Guo L, Li S. Disturbance-observer-based control and related methods-An overview. IEEE Transactions on Industrial Electronics, 2016, 63(2): 1083-1095.

[16] Chen T, Wen H. Autonomous assembly with collision avoidance of a fleet of flexible spacecraft based on disturbance observer. Acta Astronautica, 2018, 147: 86-96.

[17] Sun L, Huo W, Jiao Z. Disturbance-observer-based robust relative pose control for spacecraft rendezvous and proximity operations under input saturation. IEEE Transactions on Aerospace and Electronic Systems, 2018, 54(4): 1605-1617.

[18] Liu C, Vukovich G, Sun Z, et al. Observer-Based Fault-Tolerant Attitude Control for Spacecraft with Input Delay. Journal of Guidance, Control, and Dynamics, 2018, 41(9): 2041-2053.

[19] Weiss A, Kolmanovsky I, Bernstein D S, et al. Inertia-free spacecraft attitude control using reaction wheels. Journal of Guidance, Control, and Dynamics, 2013, 36(5): 1425-1439.

[20] Schweighart, SA. Electromagnetic Formation Flight-Dipole Solution Planning. Ph.D. Thesis, Massachusetts Institute of Technology, June 2005: 26, 42-43.

[21] Chen T, Shan J. Distributed tracking of a class of under-actuated Lagrangian systems with uncertain parameters and actuator faults. IEEE Transactions on Industrial Electronics, 2019, doi: 10.1109/TIE.2019.2922943.

[22] Zhang J, Ye D, Sun Z, et al. Extended state observer based robust adaptive control on SE(3) for coupled spacecraft tracking maneuver with actuator saturation and misalignment. Acta Astronautica, 2018, 143: 221-233.

[23] You L, Dong Y. Near time-optimal controller based on analytical trajectory planning algorithm for satellite attitude maneuver. Aerospace Science and Technology, 2019, 84: 497-509.

[24] Chen T, Shan J. Distributed control of multiple flexible manipulators with unknown disturbances and dead-zone input. IEEE Transactions on Industrial Electronics, 2019, doi: 10.1109/TIE.2019.2955417.

[25] Huang S, Yang G. Fault tolerant controller design for t–s fuzzy systems with time-varying delay and actuator fault: a k-step fault-estimation approach. IEEE Transactions on Fuzzy Systems, 2014, 22(6): 1526-1540.

[26] Shi P, Liu M & Zhang L. Fault-tolerant sliding-mode-observer synthesis of Markovian jump systems using quantized measurements. IEEE Transactions on Industrial Electronics, 2015, 62(9): 5910-5918.

[27] Shi K, Liu C, Sun Z, et al. A novel robust non-fragile control approach for a class of uncertain linear systems with input constraints. Transactions of the Institute of Measurement and Control, 2019, 41(8): 2365-2373.

[28] Tabatabaeipour SM, Bak T. Robust observer-based fault estimation and accommodation of discrete-time piecewise linear systems. Journal of the Franklin Institute, 2014, 51(1): 277-295.

[29] Liu C, Sun Z, Shi K, et al. Robust dynamic output feedback control for attitude stabilization of spacecraft with nonlinear perturbations. Aerospace Science and Technology, 2017, 64: 102-121.

[30] Yang C D, Sun Y P. Mixed H_2/H_∞ state-feedback design for microsatellite attitude control. Control Engineering Practice, 2002, 10(9): 951-970.